

Practical parameter identifiability of respiratory mechanics in the extremely preterm infant

Richard Foster¹, Laura Ellwein Fix¹

Abstract

The complexity of mathematical models describing respiratory mechanics has grown in recent years, however, parameter identifiability of such models has only been studied in the last decade in the context of observable data. This study investigates parameter identifiability of a nonlinear respiratory mechanics model tuned to the physiology of an extremely preterm infant, using global Morris screening, local deterministic sensitivity analysis, and singular value decomposition-based subset selection. The model predicts airflow and dynamic pulmonary volumes and pressures under varying levels of continuous positive airway pressure, and a range of parameters characterizing both surfactant-treated and surfactant-deficient lung. Sensitivity analyses indicated eleven parameters influence model outputs over the range of continuous positive airway pressure and lung health scenarios. The model was adapted to data from a spontaneously breathing 1 kg infant using gradient-based optimization to estimate the parameter subset characterizing the patient's state of health.

1. Introduction

Respiratory mechanics have been investigated mathematically for several decades using differential equations models that typically predict air pressure and flow in and between compartments representing aggregate features of the respiratory system. Models have grown in complexity from early compartmental models of dynamic volumes and pressures in the airways, lungs, chest wall, and intrapleural space [1]. Successive models have built upon this foundation by including nonlinear resistances and compliances, viscoelastic components, and pulmonary circulation [2, 3, 4], and more recently been adapted to newborn animal physiology [5]. We previously developed a dynamic nonlinear computational model of infant respiratory mechanics parameterized for the extremely preterm human infant [6] to propose a mechanism of delayed progressive lung volume loss attributed to high chest wall compliance (floppiness) [7, 8, 9]. Our model was the first known attempt to represent these dynamics in premature infants, and also depict the mitigating effects of expiratory laryngeal braking (grunting) and continuous positive airway pressure (CPAP) under simulated high and low chest wall compliance conditions. However, the parameter space contributing overall to breathing dynamics was not explored. Investigation of

this fragile demographic is hampered by the challenges associated with clinical data acquisition in a stabilized but extremely preterm infant. Given that ventilation assistance continues to fail in this population and with unknown etiology, this remains an area of continued study [10, 11, 12].

Forward model simulations using parameter values obtained from experiments or population-based averages provide insight into overall dynamics of a group, but estimating patient-specific parameters requires an optimization algorithm to solve an inverse problem with experimental data. In nonlinear physiological systems with large parameter spaces and a scarcity of data, the optimization problem comes with two inherent challenges for obtaining unique parameter values. The first is parameter *sensitivity*, the impact of variation in parameter values on associated model output. A sensitivity analysis can examine the small local changes around each nominal parameter value or the global variability throughout the admissible parameter space [13, 14, 5, 15, 16, 17]. Parameter values may be only valid in a local region, and may affect sensitivities of other parameters in a nonlinear system. The second challenge is parameter *identifiability*, either due to the structure of the model (structural) or the availability of data (practical) [15, 16, 18, 17]. In an example of structural unidentifiability, two or more parameters may impact an output in combination (e.g. resistors in series), but determining which parameter had the effect based on the change in output is not possible. Questions regarding parameter identifiability in a pulmonary mechanics model are especially critical in the context of typical clinical data, which for assessment of respiratory mechanics may include only the two dynamic scalar waveforms of volumetric airflow as measured by a pneumotachograph, and pleural pressure as estimated by a pressure transducer in the esophagus. Data acquired under different experimental conditions makes it possible that a waveform from one of the two outputs may change significantly but the other output may show negligible differences, or waveforms may be similar between conditions but mask different underlying dynamics. It is therefore critical to investigate which parameters most influence the model outputs under which conditions, and if any parameter dependencies exist that may allow for simplifying model components.

Parameter sensitivity analysis and estimation have been used in previous respiratory and other physiological modeling efforts, with the question of identifiability being explored more recently. However, prior studies focused on simpler linear models in a healthy adult and did not widely address the challenges involved with nonlinear models, non-adult populations, or clinical scenarios. Some of the earliest parameter estimation was performed in several linear respiratory mechanics models [19, 2, 20, 21]. Schranz et al [22, 23, 24] applied structural and practical identifiability together with parameter estimation techniques to first-order, viscoelastic, and recruitment models of respiratory mechanics and associated data, but these models represented only a lumped alveolar compartment. In the multi-compartment model of breathing in newborn lambs of Le Rolle et al [5], the parameter space was explored with Morris screening with respect to flow and pressure outputs including under a continuous positive pressure maneuver. Eight parameters were then estimated per animal using an

evolutionary algorithm and continuous time data. A similar approach was used in their follow-up study on an integrated cardiorespiratory model [25] which investigated the effects of CPAP on cardiac metrics. While these studies are a few of the only neonatal compartmental models of breathing evident in the literature, it is noted that the model parameters were linear, and the effects of CPAP on respiratory parameter sensitivity and implications of lung health were not considered.

While the computational model developed by Ellwein Fix et al [6] attempted a nonlinear compliance parameterization and demonstrated respiratory dynamics in premature infants, there was no investigation of sensitivity of the parameter space. Foster et al [26] applied global screening and local sensitivity analyses to a modified model of thoracoabdominal asynchrony, but that model and analysis were for the different purpose of determining parameters influential on phase angle under a variety of conditions. Similarly, Luke et al [27] applied parameter inference and model reduction to a simpler compartmental model against a collection of ventilator-induced lung injury pressure-volume curves from rat pups. However, the model did not consider the effects of the chest wall, the data was quasi-static and did not represent spontaneous non-ventilated breathing, and the parameterization for rat pups did not explicitly represent the human preterm infant. Despite recent progress, there remains an opportunity for parameter identification studies specific to nonlinear respiratory mechanics in the preterm infant under clinical conditions.

In this study, we propose a reduced respiratory mechanics model based on one previously developed [6] to predict the effect of multiple levels of continuous positive airway pressure (CPAP) on airflow and pleural pressure dynamics of spontaneous breathing in a 1 kg infant. Novelty in this study comes from the analysis of two different scenarios of lung health common to this demographic, surfactant-treated and surfactant-deficient, defined by distinctly different parameter subsets. To assess global parameter influence and dependencies, we applied Morris screening to parameter ranges that encompass both health scenarios and a clinical range of CPAP. Non-influential components were removed based on Morris results, and the resulting reduced model underwent local derivative-based sensitivity analysis and singular value decomposition (SVD)-based subset selection applied to each health scenario separately over the range of CPAP. Parameter estimation of the resulting sensitive, identifiable parameter set was illustrated with optimizing against clinical waveform data extracted from Abbasi and Bhutani (1990)[28]. Optimized parameter values were used to hypothesize about the lung health of the corresponding patient.

2. Model

The respiratory mechanics model is represented by lumped-parameter hydraulic compartments describing upper airways (u), intermediate collapsible airways (c), small peripheral airways (s), lungs/alveoli (A), intrapleural space (pl), and chest wall (cw). The lungs are further comprised of elastic (el) and a viscoelastic (ve) tissue separated in the model by a tissue pressure (T). The

model is similar to that developed in previous work [6] including the same system of dynamic equations. In this study, the lung recruitment constitutive relation is simplified, and additional constitutive relations are further reduced based on global parameter screening. Following is a description of the state equations, modifications to the constitutive relations, and the nominal parameterization.

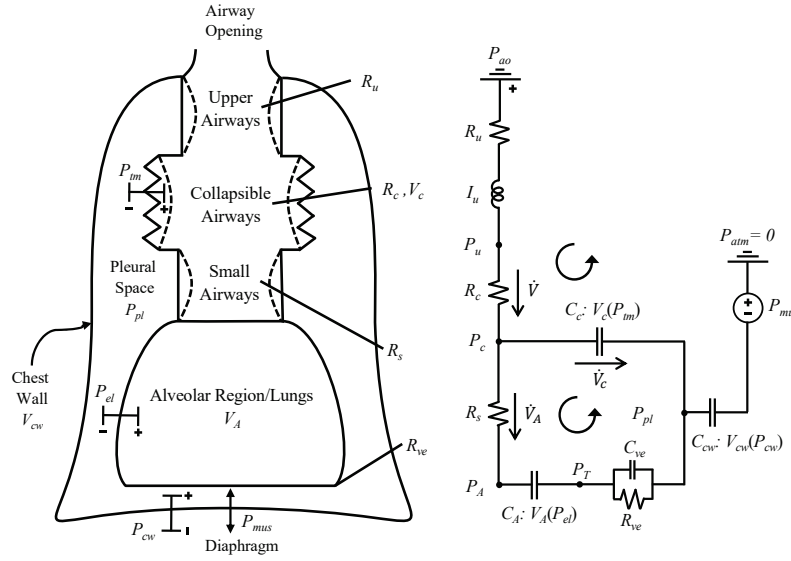


Figure 1: Lumped-parameter respiratory mechanics model (left) shown with the electrical analog (right), adapted from Ellwein Fix et al [6]. Each compliant compartment C has an associated volume V as a function of the pressures P across the compartment boundaries. Airflows \dot{V} across resistances R and inertance I are positive in the direction of the arrows. Circular arrows indicate direction of loop summations used to derive the system of differential equations (Eq. 1). Subscripts: airway opening ao , upper u , collapsible c , small peripheral s , alveolar A , viscoelastic ve , lung elastic el , tissue T , transmural tm , pleural pl , chest wall cw , muscle mus .

2.1. State equations

The hydraulic-electric circuit is used to describe dynamic volumes $V(t)$ [ml] and pressures $P(t)$ [cmH₂O] within compartments, see Fig. 1 and Table 1. This modeling construct has been used extensively in previous studies in the literature, e.g. [1, 3, 4, 5, 29]. In this style of model, intra-compartment pressures $P_i(t)$ are defined relative to the external atmospheric pressure $P_{ext} = 0$, and inter-compartment pressures are defined as the difference between two compartments $P_{ij} = P_i - P_j$ where j is downstream from i . Volume rate of change and airflow

are represented as $\frac{dV}{dt}$ and $\dot{V}(t)$ [ml/s] depending on the context. Airflow and pressure gradients are positive in the inward (hydraulic) or counter-clockwise (circuit) direction.

Table 1: Descriptions of pressure and volume state variables with units.

State	Units	Physiologic description
V	[ml]	Total volume
V_A	[ml]	Alveolar volume
V_c	[ml]	Collapsible airways volume
V_{cw}	[ml]	Chest wall volume
\dot{V}	[ml/s]	Total Airflow
P_u	[cmH ₂ O]	Upper airway pressure
P_c	[cmH ₂ O]	Collapsible airways pressure
P_A	[cmH ₂ O]	Alveolar pressure
P_T	[cmH ₂ O]	Lung tissue pressure
P_{pl}	[cmH ₂ O]	Pleural pressure
P_{el}	[cmH ₂ O]	Lung elastic recoil
P_{ve}	[cmH ₂ O]	Viscoelastic pressure of lung
P_l	[cmH ₂ O]	Total lung pressure
P_{tm}	[cmH ₂ O]	Transmural pressure across collapsible airways
P_{cw}	[cmH ₂ O]	Chest wall elastic recoil pressure
P_{mus}	[cmH ₂ O]	Total diaphragm muscle pressure

The compliant compartments, including the collapsible airways, alveoli, and chest wall, have an associated V_i and compliance C_i such that $C_i = \partial V_i / \partial P_{ij}$. Since volumes and pressures are dynamic with respect to time but compliance is not, compliance C_i can be redefined as $\dot{V}_i = C_i \dot{P}_{ij}$. Inter-compartment pressures across compliant boundaries include lung elastic recoil pressure $P_{el} = P_A - P_T$, lung viscoelastic pressure $P_{ve} = P_T - P_{pl}$, transmural airway pressure $P_{tm} = P_c - P_{pl}$, and chest wall recoil pressure $P_{cw} = P_{pl} - P_{mus}$. Kirchhoff's loop rule requires that pressure is conserved around each of the three closed loops of the electrical circuit in Fig. 1, giving the following pressure sums:

$$\begin{aligned}
0 &= (P_{atm} - P_{ao}) + (P_{ao} - P_u) + (P_u - P_c) + (P_c - P_{pl}) + (P_{pl} - P_{mus}) + P_{mus} \\
0 &= (P_c - P_A) + (P_A - P_T) + (P_T - P_{pl}) + (P_{pl} - P_c) \\
0 &= (P_T - P_{pl}) + (P_{pl} - P_T)
\end{aligned}$$

which can be written concisely with inter-compartment pressures as

$$\begin{aligned}
0 &= -P_{ao} + (P_{ao} - P_u) + (P_u - P_c) + P_{tm} + P_{cw} + P_{mus} \\
0 &= (P_c - P_A) + P_{el} + P_{ve} - P_{tm} \\
0 &= (P_T - P_{pl}) - P_{ve}
\end{aligned}$$

Pressure drops across resistances R_i [cmH₂O·s/ml] and inertance I_i [cmH₂O·s²/ml] are defined as typical circuit components with respect to air flows \dot{V}_i and acceleration \ddot{V} :

$$\begin{aligned} P_{ao} - P_u &= R_u \dot{V} + I_u \ddot{V} \\ P_u - P_c &= R_c \dot{V} \\ P_c - P_A &= R_s \dot{V}_A \\ P_T - P_{pl} &= R_{ve} \dot{V}_{ve} \end{aligned}$$

The total system volume V is equivalent to the chest wall volume, modeled as the sum of the alveolar and compressible airway volumes: $V = V_{cw} = V_A + V_c$. Kirchhoff's junction law requires that volume flow is conserved such that $\dot{V} = \dot{V}_A + \dot{V}_c$, where V_c is the volume change of the collapsible airway.

Incorporating compliance, resistance, and inertance relationships into the pressure sums gives

$$\begin{aligned} 0 &= -P_{ao} + R_u \dot{V} + I_u \ddot{V} + R_c \dot{V} + P_{tm} + P_{cw} + P_{mus} \\ 0 &= R_s \dot{V}_A + P_{el} + P_{ve} - P_{tm} \\ 0 &= R_{ve}(\dot{V}_A - \dot{V}_{ve}) - P_{ve} \end{aligned}$$

Reformulating \dot{V}_{ve} in terms of its dynamic compliant state gives the final system of loop equations:

$$\begin{aligned} 0 &= P_{ao} - R_u \dot{V} - I_u \ddot{V} + R_c \dot{V} + P_{tm} + P_{cw} + P_{mus} \\ 0 &= R_s \dot{V}_A + P_{el} + P_{ve} - P_{tm} \\ 0 &= R_{ve}(\dot{V}_A - C_{ve} \dot{P}_{ve}) - P_{ve} \end{aligned}$$

Rearranging the loop equations in terms of their derivatives gives the final system of differential equations.

$$\begin{aligned} \ddot{V} &: \frac{d\dot{V}}{dt} = \frac{1}{I_u} \left(P_{ao} - R_c \dot{V} - P_{tm} - P_{cw} - P_{mus} - R_u \dot{V} \right) \quad (1) \\ \dot{V}_c &: \frac{dV_c}{dt} = \dot{V} - \dot{V}_A = \dot{V} - \frac{1}{R_s} (P_{tm} - P_{el} - P_{ve}) \\ \dot{P}_{el} &: \frac{dP_{el}}{dt} = \frac{\dot{V}_A}{C_A} \\ \dot{P}_{ve} &: \frac{dP_{ve}}{dt} = \frac{\dot{V}_A - (P_{ve}/R_{ve})}{C_{ve}}. \end{aligned}$$

Section 22.2 introduces nonlinear constitutive relations for states such as $R_c, R_u, P_{tm}, P_{cw}, P_{el}$ and P_{mus} that preserve the well-defined structure of the system.

2.2. Constitutive relations

Resistances and pressure-volume relations defining compliances assume nonlinear formulations in the initial model, summarized in Table 2. These relations are equivalent to those used in [6], except for the representation of the recruitment function F_{rec} . Previously, in the manner of Hamlington et al [30, 6], a fraction of alveoli permanently open at zero pressure and a maximum recruitment fraction were specified. In the current study, we presume that maximum recruitment fraction is 1, and a zero pressure fraction is not prescribed but occurs naturally as a result of mean and range of opening pressures. Parameter descriptions are given in Table 3. The quantity C_A used directly in the state equations 1 is calculated exactly using symbolic computation as $C_A = \partial V_A / \partial P_{el}$. During spontaneous breathing and no ventilation support, the airway opening pressure P_{ao} is set to 0 cmH₂O. The diaphragm muscle pressure $P_{mus}(t)$ connected to the chest wall simulates respiratory muscle activation with a sinusoidal pressure signal.

Table 2: Nonlinear resistance and pressure-volume (compliance) constitutive relations. See Ellwein Fix et al [6] for detailed descriptions.

Description	Constitutive Relation
Upper airways resistance	$R_u(\dot{V}) = R_{um} + K_u \dot{V} $
Collapsible airways resistance	$R_c(V_c) = K_c \left(\frac{V_{c,max}}{V_c} \right)^2$
Small (peripheral) airways resistance	$R_s(V_A) = R_{sd} \cdot e^{K_s(V_A - RV)/(TLC - RV)} + R_{sm}, \quad K_s < 0$
Collapsible airways pressure-volume	$V_c(P_{tm}) = \frac{V_{c,max}}{1 + e^{-(P_{tm} - c_c)/d_c}}$
Chest wall pressure-volume	$V_{cw}(P_{cw}) = RV + b_{cw} \ln \left(1 + e^{(P_{cw} - c_{cw})/d_{cw}} \right),$ where $V_{cw}(0) = RV + \nu \cdot VC$ and $b_{cw} = \frac{\nu \cdot VC}{\ln(e^{-c_{cw}/d_{cw}} + 1)}.$
Lung pressure-volume	$V_A(P_{el}) = V_{el}(P_{el}) \cdot F_{rec}(P_{el}) + RV,$ where $V_{el} = VC \cdot (1 - e^{(-kP_{el})})$ and $F_{rec} = \frac{1}{1 + e^{-(P_{el} - c_F)/d_F}}.$
Diaphragm muscle driving pressure	$P_{mus}(t) = A_{mus} \cos(2\pi ft) - A_{mus}$

2.3. Parameterization

Nominal parameter values for model equations in Eq. 1 and Table 2, shown in Table 3, comprise the full parameter set θ . Parameter values are the same for surfactant-treated and surfactant-deficient lung scenarios except for the parameter set $\{TLC, k, c_F, d_F\}$. Airway opening pressure P_{ao} is considered a parameter for sensitivity analyses and varies with CPAP level. Further details are given below.

2.3.1. Lung scenarios

Surfactant-treated lung ("treated"). Parameters were manually tuned based on literature reference values such that resulting lung and chest wall compliance curves produced dynamics comparable to key scalar quantities reported for a 1 kg infant with a surfactant-treated lung, a typically underdeveloped and highly

Table 3: Parameter descriptions and nominal values for “healthy” surfactant-treated lung, a highly compliant rib cage, and no ventilatory support.

Parameter	Units	Baseline Value	Physiological Description	References
TLC	[ml]	63	Total lung capacity	[31, 32]
RV	[ml]	23	Residual volume	[31]
VC	[ml]	40	Vital capacity, TLC-RV	[31, 32]
RR	[br/min]	60	Respiratory rate	[32]
f	[br/s]	1	Respiratory frequency, RR/60	—
T	[s]	1	Duration of respiratory cycle, $1/f$	—
A_{mus}	[cmH ₂ O]	1.85	Breathing muscle pressure amplitude	—
R_{um}	[cmH ₂ O/L/s]	20	Upper airway resistance minimum value	[33, 34]
K_u	[cmH ₂ O/L ² /s ²]	60	Upper airway resistance flow-dependent coefficient	[33, 4, 34]
I_u	[cmH ₂ O/L/s ²]	0.33	Upper airway inertance	[34, 5]
$V_{c,max}$	[ml]	2.5	Collapsible airway maximum volume	estimated as dead space [32, 35]
K_c	[cmH ₂ O/L/s]	0.1	Collapsible airway resistance volume-dependent coefficient	estimated from adult [4]
R_{sm}	[cmH ₂ O/L/s]	12	Small airway resistance minimum	[36, 34]
R_{sd}	[cmH ₂ O/L/s]	20	Small airway resistance difference	[4]
K_s	unitless	-15	Small airway resistance volume-dependent coefficient	[4]
c_c	[cmH ₂ O]	4.4	Collapsible airway pressure at maximum compliance	[3]
d_c	[cmH ₂ O]	4.4	Collapsible airway pressure range coefficient	[3]
k	[1/cmH ₂ O]	0.07	Lung elasticity pressure-dependent coefficient	[37, 30]
c_F	[cmH ₂ O]	0.1	Lung recruitment mean opening pressure	[30]
d_F	[cmH ₂ O]	0.4	Lung recruitment pressure range coefficient	[30]
c_{cw}	[cmH ₂ O]	0	Transition pressure, chest wall pressure-volume	—
d_{cw}	[cmH ₂ O]	0.48	Chest wall pressure-volume slope coefficient	—
ν	[ml]	0.25	Chest wall relaxation volume coefficient	[32, 38]
C_{ve}	[ml/cmH ₂ O]	0.005	Lung viscoelastic compliance	[4]
R_{ve}	[cmH ₂ O/L/s]	20	Lung viscoelastic resistance	[4]
$P_{a,o}$	[cmH ₂ O]	0	Airway opening pressure	

compliant (floppy) rib cage, and no ventilatory support [6]. Several key clinical scalar quantities were calculated and compared against literature average values to facilitate parameter tuning. Table 4 reports values for these scalar quantities and references for comparison to literature. Functional residual capacity (FRC) was calculated using a nonlinear solver as the volume where static chest wall pressure P_{cw} balanced against lung elastic pressure P_{el} , such that $P_{cw}|_{FRC} + P_{el}|_{FRC} = 0$. Tidal volume V_T was calculated as the difference between maximum and minimum lung volume V_A during a single tidal breathing cycle, such that $V_T = \max(V_A) - \min(V_A)$. Minute ventilation, a scalar that describes how much air enters the respiratory system within one minute \dot{V}_E [32] was calculated as tidal volume V_T times respiratory rate RR. Breath-to-breath dynamic chest wall compliance $C_{cw,dyn}$ and dynamic lung compliance $C_{l,dyn}$ were calculated during a single breath with the following definitions:

$$C_{cw,dyn} = \frac{\max(V_{cw}) - \min(V_{cw})}{\max(P_{cw}) - \min(P_{cw})} \quad \text{and} \quad C_{l,dyn} = \frac{\max(V_A) - \min(V_A)}{\max(P_{el}) - \min(P_{el})}. \quad (2)$$

Chest wall compliance is nearly 4 times higher than lung compliance, appropriate for a preterm infant [39].

Table 4: Model and literature reported scalar quantities referenced for nominal parameter tuning.

Output	Model value	References
FRC	24.9 ml	[31, 32, 40]
V_T	6 ml	[41, 42, 43]
\dot{V}_E	360 ml/min	[32]
$C_{l,dyn}$	2.56 ml/cmH ₂ O	[39, 33, 41]
$C_{cw,dyn}$	9.9 ml/cmH ₂ O	[39, 33]

Surfactant-deficient lung ("deficient"). The surfactant-deficient lung may have evidence of microatelectasis, or diffuse lung collapse, possibly as a result of insufficient surfactant or other stabilizing forces in the chest wall. In the model, this is described by one or more of the following characteristics: lower TLC, lower elasticity k , higher mean opening pressure c_F , and larger range of opening pressures d_F . These manifest in the pressure-volume curve as lower volumes with respect to alveolar pressure and a right-ward shift of the sigmoidal function F_{rec} in the positive pressure range. In this study, the surfactant deficient lung is modeled by decreasing k and TLC and increasing c_F and d_F (see Table 5). Fig. 2 shows the recruitment relations and static pressure-volume curves for both treated and deficient lungs over a wide range of lung elastic recoil pressures, P_{el} . The treated lung recruitment function exhibits a clear distinction between minimum and maximum recruitment at small pressures due to small c_F and d_F , leading to higher breath-to-breath dynamic lung compliances $C_{l,dyn}$ at low

P_{el} pressures. The deficient lung exhibits reduced lung recruitment over a wide range of P_{el} due to an increase in c_F and d_F . When combined with the less compliant $V_{el}(P_{el})$ relation, the static lung pressure-volume relation $V_A(P_{el})$ appears more sigmoidal in construction, inducing much lower $C_{l,dyn}$ at low lung elastic recoil pressures.

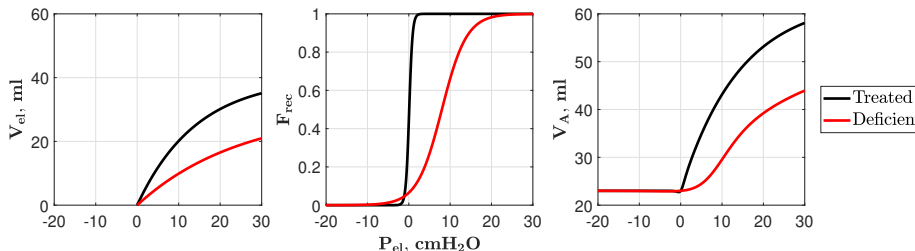


Figure 2: Lung recruitment $F_{rec}(P_{el})$ and pressure-volume relations for $V_{el}(P_{el})$ and $V_A(P_{el})$ with treated (black) and deficient (red) lung modeling scenarios. Lung elastic recoil volume $V_{el}(P_{el})$ (left) represents maximum possible lung volume before scaling by the lung recruitment $F_{rec}(P_{el})$ relation (middle) and summing residual volume RV to obtain alveolar/lung volume $V_A(P_{el})$ (right). See also Table 2 for detailed lung pressure-volume relation.

Table 5: Model parameter values for treated and deficient lungs. See Table 3 for parameter descriptions.

Parameter	Treated	Deficient
TLC	63 ml	53 ml
k	0.07 1/cmH ₂ O	0.04 1/cmH ₂ O
c_F	0.1 cmH ₂ O	8 cmH ₂ O
d_F	0.5 cmH ₂ O	3 cmH ₂ O

2.3.2. Airway opening pressure

Continuous positive airway pressure (CPAP) ventilation applies a positive pressure to the patient’s airway opening, thereby raising the pressure in the patient’s lungs to keep them open and stable. This raises end-expiratory lung volume (EELV) (equivalent to $\min(V_A)$), thereby causing tidal breathing to occur at higher lung pressures. Given the nonlinearity of the constitutive relations, we hypothesized that the application of CPAP would change the relative sensitivities of related parameters and in different ways for the treated vs deficient lung. CPAP was modeled in this study with increasing values of airway opening pressure P_{ao} , ranging from 0 to 8 cmH₂O [44, 25]. Other direct effects of CPAP, such as a lowering of upper airway resistance, were neglected unless they result from constitutive relations.

3. Data

Given the fragility of the extremely preterm infant population, it is nearly impossible to obtain clinical waveforms of airflow and pleural pressure from a spontaneously breathing, non-ventilated patient. The majority of these infants require ventilation for breathing stability, and likewise if they are stable enough not to require ventilation, they are not consented for non-critical clinical data acquisition. In a rare study from 1990, Abbasi and Bhutani [28] enrolled 33 healthy, non-ventilated, low birthweight infants (>1500 g and ≤ 34 weeks gestation) to observe and record pulmonary mechanics. The data airflow \dot{V}^d and pleural pressure P_{pl}^d waveforms from a 1 kg infant found in Fig. 1 of [28] were extracted using PlotDigitizer [45] and used in this study, shown here in Fig. 5.

4. Model Sensitivity and Identifiability

Sensitivity analyses of the parameter space were performed to show how model outputs respond to physiologically relevant ranges of parameter values under a range of CPAP settings for the model treated and deficient lungs. We first used the Morris global screening method to remove non-influential and non-interacting parameters according to key scalar model outputs. Similar to Colebank and Chesler [46] and as discussed by Campolongo et al [47], Morris screening is advantageous for large parameter spaces. Results from the screening were used for model reduction by removing or linearizing compartments. Local derivative-based sensitivity analysis was then applied to the treated and deficient lung reduced parameter spaces according to airflow and esophageal pressure time-dependent outputs, for a range of P_{ao} emulating CPAP. Sensitive parameters were further analyzed for identifiability with an SVD-based subset selection method [48] similar to methods used by Dadashova et al [49]. Model outputs for all aforementioned sensitivity and identifiability analyses were obtained by solving the system in Eq. 1 with the built-in differential equations solver ode15s in MATLAB 2024b. Absolute and relative tolerances for the solver were fixed at $1e-8$, and the Jacobian finite difference approximation increment used later in subset selection was set to $1e-4$, defined as the square root of the solver tolerance. Time steps were set to 0.002 seconds, and initial conditions for \dot{V} , V_c , and P_{ve} were fixed at 0 ml/s, 0.1 ml, and 0 cmH₂O, respectively. The initial condition for P_{el} was set as the lung elastic recoil pressure at functional residual capacity. Further information about the computational model architecture can be found in Appendix A, with full code provided in Data Availability.

4.1. Morris Screening

The Morris method [50, 51] measures the coarse derivative approximation, or “elementary effect”, of each parameter of interest θ_j vs a scalar output of interest. The method adjusts one parameter at a time by a scaled step-size Δ , generates a model solution, then calculates an elementary effect, repeated for a prescribed finite number of runs. The mean μ_j and variance σ_j^2 of the

elementary effects for each parameter is calculated, and the Morris index, defined as $M_j = \sqrt{\mu_j^2 + \sigma_j^2}$, ranks parameters by overall influence on scalar model output. Large μ_j demonstrate that the j^{th} parameter has heavy influence on model output, and large σ_j^2 demonstrate high nonlinearity or interaction with other parameters [51, 52]. The computational implementation was based on one developed by Colebank and Chesler [46] and used in Foster et al [26]. Further details regarding the computational scheme can be found in [53, 54].

Parameter space bounds (Table 6) were chosen to be either a feasible physiological range, or $\pm 50\%$ if such a range was unknown. In particular, the upper bounds on c_F and d_F represent a high mean opening pressure and a range of opening pressures such as may occur in a deficient lung. Also P_{ao} extends to a feasible clinical range, to ensure that extremes of CPAP were captured. Morris indices M_j are used to first reduce the model by removal of non-influential parameters, and then set up the parameter set θ_{sens} on which local sensitivity analysis is applied.

4.2. Local sensitivity analysis

A single model output is described by the vector:

$$y = [y_p(t_1; \theta), \dots, y_p(t_{N_i}; \theta)]^T \quad (3)$$

where N_i is the number of time points in a single breathing cycle and θ is the vector of parameters of length N_j . Model outputs correspond to data waveforms and thus can be a combination of $y_1 = \dot{V}(t)$ and $y_2 = P_{pl}(t)$, where \dot{V} is a state variable of Eq. 1, and P_{pl} is calculated from state variable P_{el} through several constitutive relations. If both \dot{V} and P_{pl} outputs are analyzed, they are concatenated, giving y length $2N_i$. We applied a gradient-based approach [13, 52] to calculate time-dependent sensitivities for each simulation and parameter, around nominal values θ^* for treated and deficient scenarios. A steady-state full cycle was used to ensure that transient behavior was excluded.

First the output(s) of y are scaled by their maximum absolute value y_{max} (avoiding division by small numbers),

$$\hat{y} = \left[\frac{y(t_1; \theta)}{y_{max}}, \dots, \frac{y(t_{N_i}; \theta)}{y_{max}} \right]^T \quad (4)$$

Columns \hat{S}_j of the $N_i \times N_j$ relative sensitivity matrix \hat{S} are determined by differentiating \hat{y} and multiplying by the nominal parameter value θ_j [55, 14, 56]:

$$\hat{S}_j(t; \theta_j) \Big|_{\theta_j = \theta_j^*} = \theta_j \frac{\partial \hat{y}(t; \theta_j)}{\partial \theta_j} \Big|_{\theta_j = \theta_j^*}. \quad (5)$$

Derivatives of \hat{y} with respect to θ_j were computed with a forward difference approximation using a difference increment of $\epsilon_j = 1e-4$ [57, 48]. To obtain a

composite value for ranking, we computed a 2-norm sensitivity S_j across the pN_i -size column of \hat{S} for each parameter:

$$S_j = \left\| \hat{S}_j \right\|_2. \quad (6)$$

A parameter is considered to be the "sensitive" set for a given lung scenario or CPAP level based on two possible criteria: Quantitatively, the composite sensitivity is greater than the tolerance of the forward difference scheme, or qualitatively, there is an appreciable drop-off in sensitivity when parameters are ranked. The parameter subset on which subset selection is applied is denoted as θ_{sub} .

4.3. Subset selection

We applied a subset selection method based on singular value decomposition and QR factorization [48, 49] to further address practical identifiability of the sensitive parameter set given the two clinically relevant outputs [58]. We began by computing the singular value decomposition of the sensitivity matrix $\hat{S}|_{\theta=\theta^*} = U\Sigma V^T$ where Σ is a $N_i \times N_j$ diagonal matrix of singular values in decreasing order, with 0's in rows $N_i - N_j + 1$ to N_i , and V is a $N_j \times N_j$ matrix containing the corresponding right singular vectors as its columns. The numerical rank ρ indicates the number of maximally independent columns of \hat{S} , using a prescribed ϵ such that $\sigma_\rho/\sigma_1 > \epsilon \geq 10\epsilon_J$, where σ_1 is the largest singular value and ϵ_J is the set Jacobian finite difference approximation increment of length $1e-4$ (thus giving a cutoff as $1e-3$). The numerical rank is equivalent to the number of parameters that can be identified given the model output \hat{y} and is used to partition $V = [V_\rho V_{N_j-\rho}]$. The particular parameters associated with the ρ largest singular values are found using QR-decomposition with column pivoting. The permutation matrix P that results from the decomposition $V_\rho^T P = QR$ is applied to reorder the parameter vector θ^* to obtain $\tilde{\theta}^* = P^T \theta^*$, which is partitioned as $\tilde{\theta}^* = \tilde{\theta}_\rho^* \tilde{\theta}_{N_j-\rho}^*$. The vector $\theta_{opt} = \tilde{\theta}_\rho^*$ then constitutes an independent set of model parameters deemed estimable as part of a reduced-order optimization problem, introduced in Section 4.4.

4.4. Optimization

Patient-specific parameter optimization for the identifiable subset θ_{opt} was demonstrated by solving the following reduced-order problem by using data for one spontaneously breathing 1 kg infant (see Section 3):

$$\arg \min_{\theta} J(\theta_{opt}), \quad (7)$$

where J is a cost function, and parameters not found in θ_{opt} remain fixed at baseline estimates. Nominal parameter values θ^* for the treated lung were used as initial guesses. Optimization was repeated with deficient lung parameter values to determine if different starting guesses would result in a different optimized parameter set. Parameters not in θ_{opt} were kept constant at nominal

values. Given that, clinically, the patients from that study had no ventilation support, P_{ao} was set at 0 cmH₂O.

The optimization included both model outputs and data time series. The resulting cost function J is a least squares formulation using the outputs given in Section 4.4.2:

$$J = \sum_{i=1}^N \left| \frac{\dot{V}^m(t_i; \theta) - \dot{V}_i^d}{\dot{V}_{max}^d} \right|^2 + \sum_{i=1}^N \left| \frac{P_{pl}^m(t_i; \theta) - P_{pl,i}^d}{P_{pl,max}^d} \right|^2. \quad (8)$$

Superscripts d, m refer to the data and model respectively, and subscript max denotes the maximum in absolute value of each data set. A bound-constrained Levenberg-Marquardt (L-M) optimization algorithm with trust region [48, 59] and regularization parameter $\gamma = 0.2$ was used. Lower and upper bounds for parameter constraints in L-M were set at the Morris bounds, as these were chosen with the specific physiology and feasible clinical conditions in mind. Each parameter value is scaled during the optimization by the difference of the bounds for that parameter. The L-M algorithm terminates with tolerance of $1e-4$ based on gradient norm $\|\nabla J(\theta)\|$ or residual $J(\theta)$, i.e. the iteration continues until one has fallen below the tolerance for any of the convergence criteria.

4.5. Summary of Procedures

The Morris method was applied with four scalar outputs, chosen to correspond to obtainable clinical measurements:

- Tidal volume V_T
- End-expiratory lung volume $EELV \min(V_A)$
- Maximum airflow \dot{V}_{max}
- Maximum magnitude pleural pressure $|P_{pl}|_{max}$

Local sensitivity analyses and subset selection were performed on model outputs emulating possible available clinical data scenarios:

- Both airflow and pleural pressure signals: time series $\dot{V}(t), P_{pl}(t)$
- Airflow signal only: time series $\dot{V}(t)$
- Pressure signal only: time series $P_{pl}(t)$

The sequence of sensitivity analysis steps are as follows:

1. Perform Morris screening on θ for all four scalar model outputs with parameter ranges encompassing both treated and deficient lungs, for 1000 runs total. Rank Morris indices M_j for all scalar outcomes and calculate the mean \bar{M}_j and median \tilde{M}_j for each output.

2. At this initial screening we consider three tiers of influence $\theta_1, \theta_2, \theta_3$ based on previous practice [46], with θ_1 being most influential. If $M_j > \bar{M}_j$ (mean) for one or more scalar model outputs, parameter θ_j is part of the most influential tier θ_1 and considered for sensitivity analysis. If $M_j < \tilde{M}_j$ (median) for all scalar model outputs, the parameter θ_j is considered non-influential in θ_3 and is no longer analyzed. All other parameters in between are put in in θ_2 and analyzed further.
3. The initial model is reduced by linearizing nonlinear components based on removal of parameters in $\theta_2 \cup \theta_3$ from the model but retaining structure.
4. Local sensitivity analysis is applied to θ_{sens} , a subset of $\theta_1 \cup \theta_2$, with respect to simulated $\dot{V}(t)$ and $P_{pl}(t)$ from the reduced model with 5 levels of CPAP ventilatory support such that $P_{ao} = 0, 2, 4, 6, 8$ cmH₂O. Nominal parameter values are set as given in Table 3 for the treated lung and Table 5 to show the differences for the deficient lung for k , TLC, c_F , and d_F .
5. S_j are calculated per parameter for each of 5 CPAP simulations then averaged to obtain a measure of sensitivity for each parameter. The set of parameters with sensitivities higher than an apparent threshold are identified for the subset selection and referred to as θ_{sub} . S_j are also analyzed vs CPAP level to ascertain the nonlinear sensitivity dependence on P_{ao} .
6. Subset selection is applied to θ_{sub} for all outputs to discern any identifiability differences between lung health status, and selected parameters form a new set θ_{opt} .
7. Sensitive, identifiable parameters in θ_{opt} are optimized against the data set extracted from [28].

5. Results

5.1. Nominal outputs

Nominal model outputs for surfactant-treated and deficient lung scenarios with no CPAP ventilation support are shown in Fig. 3(A-D). Simulated waveforms were generated by the initial model before parameter screening, according to nominal parameter values in Table 3 and lung health parameters in Table 5. Both surfactant-treated and deficient lung scenarios were driven by the same diaphragmatic muscle pressure signal P_{mus} , with the treated lung case reporting a maximum absolute airflow $|\dot{V}|_{max}$ of 20.03 ml/s, maximum absolute pleural pressure $|P_{pl}|_{max}$ of 3.76 cmH₂O, and tidal volume V_T of 5.8 ml. Breath-to-breath dynamic lung and chest wall compliances $C_{l,dyn}$ and $C_{cw,dyn}$ were respectively reported at 2.5 and 10.3 ml/cmH₂O, close to reported scalar quantities in Table 4 and the 4:1 ratio between $C_{cw,dyn}$ and $C_{l,dyn}$. Compared to the treated lung scenario, the deficient lung model outputs reported severely suppressed airflow and tidal volume, with $|\dot{V}|_{max}$ decreasing to 4.90 ml/s and a near six-fold reduction in V_T to 0.96 ml. Similarly, $C_{l,dyn}$ observed a 10-fold decrease in value to 0.30 ml/cmH₂O, and $C_{cw,dyn}$ decreased three-fold to 3.2 ml/cmH₂O,

effectively stiffening the lung and chest wall compartment boundaries during a single breath. Maximum absolute pleural pressure $|P_{pl}|_{max}$ increased from 3.76 to 4.38 cmH₂O, initially suggesting that a stronger inter-compartment pressure exists across the lung boundary. However, this pressure gradient balanced against a stiffer lung due to a decrease in $C_{l,dyn}$, rendering any efforts to improve tidal breathing ineffective.

Static pressure-volume curves for $V_A(P_{el})$ and $V_{cw}(P_{cw})$ with treated and deficient-associated nominal parameters are presented in Fig. 3(E,F). Total respiratory system compliance is composed of the pressure-wise summation of $V_A(P_{el})$ and $V_{cw}(P_{cw})$, and FRC represents when total respiratory pressure reaches zero. Tidal breathing loops represent the dynamic trajectory of simulated alveolar volume V_A against total lung pressure $P_l = P_{el} + P_{ve}$. Hysteretic behavior in the tidal loops is caused by the viscoelastic structure of the lungs and their associated parameters R_{ve} and C_{ve} . Tidal loops are shown for P_{ao} fixed at 0 and 8 cmH₂O, characterizing total breathing dynamics with either absent or extreme CPAP ventilation support, respectively. Increasing P_{ao} from 0 to 8 cmH₂O shifts the tidal loop up the static lung pressure-volume curve. FRC was reported to be 25.1 ml in the treated lung scenario and 23.2 ml in the deficient scenario. In the treated lung scenario (E), increasing P_{ao} from 0 to 8 caused a tidal volume decrease from 5.8 to 4.5 ml. Scalar output $C_{l,dyn}$ decreased from 2.5 to 1.5 ml/cmH₂O, whereas $C_{cw,dyn}$ increased drastically from 10.3 to 24.0 ml/cmH₂O, indicating a stiffer lung and floppier chest wall within the region of tidal breathing. In the deficient lung scenario (F), an increase in P_{ao} caused an improvement in V_T from 0.96 to 3.8 ml and increased $C_{l,dyn}$ and $C_{cw,dyn}$ from 0.30 to 1.24 cmH₂O and 3.2 to 11.98 cmH₂O, respectively.

5.2. Morris screening

Parameter bounds and Morris screening results are given in Table 6. The highest tier for a parameter over all scalar model outputs was designated as its overall tier. The resulting three tiers of parameters were found to be

$$\theta_1 = \{P_{ao}, k, c_F, d_F, TLC, d_{cw}, A_{mus}, RV, RR\}, \quad (9)$$

$$\theta_2 = \{R_{um}, R_{ve}, \nu, R_{sm}, V_{c,max}\}, \quad (10)$$

and

$$\theta_3 = \{c_c, d_c, R_{sd}, K_s, K_u, I_u, K_c, C_{ve}\}. \quad (11)$$

The set θ_1 was retained in the model as influential, therefore it was not considered for model reduction. The tier with the lowest overall indices θ_3 was deemed non-influential, so parameters in θ_3 were not further analyzed for sensitivity but considered for model reduction. Parameters in the second tier θ_2 are connected to parameters in the first and third tiers through constitutive relations and must be explored further.

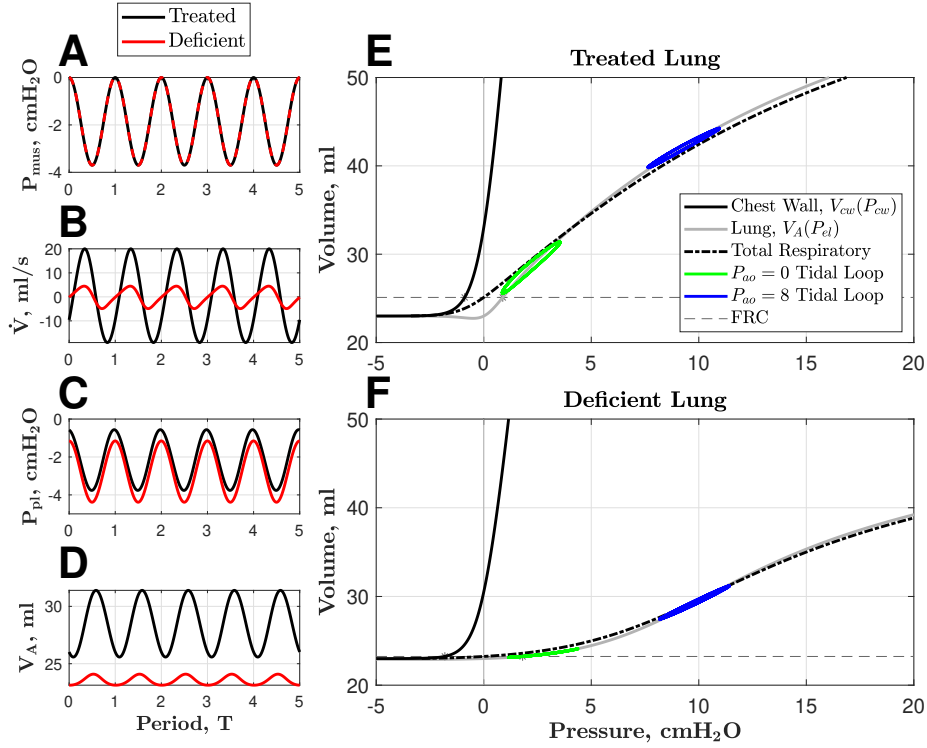


Figure 3: Steady-state waveforms of model outputs with nominal parameter sets for the surfactant-treated and deficient lung scenarios (panels A-D) and static pressure-volume curves for the alveolar/lung region, chest wall, and total respiratory system (panels E-F). Dynamic model outputs include total diaphragm muscle pressure P_{mus} , airflow \dot{V} , pleural pressure P_{pl} , and alveolar/lung volume V_A over five continuous breaths. Chest wall $V_{cw}(P_{cw})$ and lung $V_A(P_{el})$ pressure-volume relations sum pressure-wise to form total respiratory compliance. Tidal loops are represented as alveolar/lung volume $V_A(P_l)$ with fixed P_{ao} values of 0 (green) and 8 (blue) cmH₂O, where P_l represents total lung pressure ($P_{el} + P_{ve}$). Functional residual capacity (FRC) is depicted as the volume at which the total respiratory system is at rest, or when respiratory pressure is equivalent to atmospheric pressure.

5.3. Model reduction

The initial model was reduced based on removal or consolidation of parameters in the set $\theta_2 \cup \theta_3$. After observing all compartments may contribute non-trivially to the system dynamics, the nonlinear portions of several non-influential compartments were linearized instead of removed to maintain model structure. Parameters $R_{um}, K_u, K_c, V_{c,max}, R_{sm}, R_{sd}, K_s$ characterized the upper, collapsible, and small airway resistances and were not contained in θ_1 . Recognizing that resistances are essential to the system dynamics, each nonlinear resistance was replaced by a single constant value for R_u, R_c, R_s . Parameters $R_{um}, K_u, K_c, R_{sm}, K_s$, and R_{sd} were removed from the remainder of the study. Constant resistances R_u, R_c , and R_s were given nominal values of 20, 0.6, and 12 cmH₂O, respectively, informed by average resistance values during tidal breath-

Table 6: Parameter bounds and screening results for Morris sensitivity analysis. 1: Tier one, above the average. 2: Tier 2, below the average but above the median. The highest tier for a parameter over all scalar model outputs was given as its overall tier. Parameters for which the index was never above the median fell into tier 3. Scalar Outputs: V_T , tidal volume; EELV, end-expiratory lung volume; \dot{V}_{max} , peak airflow; $|P_{pl}|_{max}$, peak magnitude plural pressure. See Table 3 for parameter descriptions.

Parameter	Bounds	V_T	EELV	\dot{V}_{max}	$ P_{pl} _{max}$	Morris subset
P_{ao}	[0.01,8]	1	1	1	1	1
k	[0.04,0.07]	1	1	1	1	1
c_F	[0.1,8]	1	1	1	1	1
d_F	[0.5,3]	1	1	1	1	1
TLC	[53,73]	1	1	1	2	1
d_{cw}	[0.48,2.4]	1	2	1	1	1
A_{mus}	[1.0,4.0]	1	2	1	1	1
RV	[20,26]	2	1	2	2	1
RR	[45,75]	2	2	1	2	1
R_{um}	[10,30]	2	2	2	2	2
R_{ve}	[10,30]	2	2	2		2
ν	[0.2,0.3]		2		2	2
R_{sm}	[6,18]	2		2		2
$V_{c,max}$	[2,3]				2	2
c_c	[3.3,5.5]					3
d_c	[3.3,5.5]					3
R_{sd}	[10,30]					3
K_s	[-20,-10]					3
K_u	[45,75]					3
I_u	[.23,.43]					3
K_c	[.05,.15]					3
C_{ve}	[.003,.007]					3

ing. Maximum collapsible airway volume $V_{c,max}$ was retained in the model due to its use in the collapsible airway pressure-volume relation, which was also retained to maintain a volume separate from alveolar volume. Inertance I_u separating resistances R_u and R_c was retained since it has been shown to be a factor in the representation of the very small airways in infant breathing [60, 5].

After consolidation and removal, parameter sets θ_2 and θ_3 were redefined as

$$\theta_2 = \{R_u, R_{ve}, \nu, R_s, V_{c,max}, R_c\} \quad (12)$$

and

$$\theta_3 = \{c_c, d_c, C_{ve}, I_u\}. \quad (13)$$

In summary, the reduced model consisted of the same differential equations as the model in Fig. 1. The constitutive relations for the airway resistances became constant, and viscoelastic resistance R_{ve} and maximum collapsible airway volume $V_{c,max}$ were retained. For the remainder of this study, we will refer to the "reduced model" as the model presented in Fig. 1 with nonlinear chest wall, collapsible airway, and lung pressure-volume relations from Table 2 and constant resistances R_u, R_c , and R_s . Local sensitivity analysis was considered for the set $\theta_1 \cup \theta_2$. Parameters in set θ_3 were not included in the local sensitivity analysis.

5.4. Local sensitivity analysis

A subset of $\theta_1 \cup \theta_2$,

$$\{RR, P_{ao}, RV, R_c\}, \quad (14)$$

was not included in the sensitivity analysis. Respiratory rate RR would be extracted from data, and P_{ao} would be a model input that mimics CPAP prescribed in the clinic. While RV may change with lung health, it is an extra degree of freedom with TLC and could theoretically be estimated *a priori* for the idealized subject. Finally, as R_c and R_u operate in series with a constant inductor, their behavior is dependent, so R_c was fixed at its nominal value since $R_c \ll R_u$. The remaining 11 parameters for sensitivity analysis on the reduced model comprise θ_{sens} :

$$\theta_{sens} = \{TLC, c_F, d_F, k, \nu, d_{cw}, A_{mus}, R_s, R_u, V_{c,max}, R_{ve}\}. \quad (15)$$

Local sensitivities defined by Eq. 6 were obtained for the parameter set θ_{sens} against combined and individual model outputs P_{pl} and \dot{V} across five levels of CPAP. All system parameters were initialized by their nominal values in Table 3, and specific nominal values for the deficient lung parameters TLC, k , c_F , and d_F are listed in Table 5.

Figure 4(A-C) shows the relative local sensitivities of θ_{sens} for each model output in the treated lung scenario. Total lung capacity TLC, lung elasticity k , upper airway resistance R_u , chest wall relaxation volume ν , driving pressure amplitude A_{mus} , small airway resistance R_s , and chest wall compliance coefficient d_{cw} were the parameters with the highest sensitivity rankings against combined airflow \dot{V} and pleural pressure P_{pl} in the treated scenario. A noticeable drop-off in sensitivity occurred where maximum compressible airway volume $V_{c,max}$, viscoelastic resistance R_{ve} , lung recruitment range coefficient d_F , and mean opening lung pressure c_F had sensitivities less than 10% of the maximally sensitive TLC. Chest wall relaxation volume, ν , was the most sensitive parameter against pleural pressure P_{pl} , but experienced a steep decrease

in sensitivity against airflow \dot{V} , whereas lung elasticity k was largely sensitive for all individual model outputs. Figure 4(D-F) shows relative sensitivities for the parameter set θ_{sens} for three model outputs in the surfactant-deficient lung scenario. Like in the treated lung scenario, total lung capacity TLC, muscle pressure amplitude A_{mus} , lung elasticity k , and chest wall compliance slope d_{cw} were found to be the most sensitive parameters against combined airflow \dot{V} and pleural pressure P_{pl} outputs. Lung compliance parameters c_F and d_F had much higher sensitivities and sensitivity rankings in the deficient lung scenario, possibly due to increased nominal values and a flat sigmoidal lung pressure-volume curve. Resistances R_u , R_s , and R_{ve} appeared to influence P_{pl} at negligible levels, and R_{ve} was least sensitive against individual and combined model outputs.

Figure 4(G-L) displays the relative local sensitivities of θ_{sens} against varying levels of CPAP for the treated and deficient lung modeling scenarios. Relative sensitivities for ν and k were directly related to administered CPAP level against pleural pressure P_{pl} , whereas parameters TLC and k are inversely associated with CPAP level against airflow \dot{V} . Furthermore, parameters A_{mus} and d_{cw} displayed an decrease and subsequent increase in relative sensitivity against P_{pl} as P_{ao} increased, indicating preferential influence on model output at either absent or extreme levels of CPAP administration. Parameters $V_{c,max}$ and R_{ve} showed negligible sensitivity against all model outputs and CPAP levels in the treated lung scenario. Resistances R_u and R_s were insensitive towards P_{pl} but highly sensitive towards \dot{V} , with little change in contribution as P_{ao} increased. When CPAP was not being administered, total lung capacity, lung elasticity, and upper airway resistance were the most sensitive factors in determining pleural pressure and airflow outputs in a treated lung scenario. Parameter impact on the combined model output was generally dominated by impact on airflow. In the deficient lung scenario (panels J-L), sensitivities for TLC and k became directly related to CPAP level P_{ao} against combined outputs, contrasted with the treated lung. Mean opening lung pressure c_F became the second most sensitive parameter at intermediate values of CPAP against combined model outputs, largely determined by its impact on airflow. Muscle pressure amplitude A_{mus} and chest wall pressure-volume slope d_{cw} both showed a significant drop in sensitivity against combined outputs as CPAP increased in the deficient lung scenario, suggesting that chest wall-associated inputs matter less in determining outputs when CPAP is administered.

Table 7 shows parameter rankings of θ_{sens} according to mean relative sensitivity index against individual and combined model outputs P_{pl} and \dot{V} , corresponding to the mean (black) line in Fig. 4(A-F). Parameters TLC, k , and A_{mus} were, on average, the three most sensitive parameters across all modeling scenarios and outputs, whereas parameters c_F and d_F became markedly more influential towards deficient model outputs. Relative sensitivities and rankings for $V_{c,max}$ were close to the lowest for the combined model output, but it became moderately sensitive against P_{pl} . Viscoelastic resistance R_{ve} was consistently the lowest sensitivity parameter for the deficient lung, with slightly more sensitivity in the treated lung. While these results might suggest naming the lowest

ranking parameters as insensitive, all sensitivities are higher than the finite difference discretization of $1e - 4$. We theorize that any parameters that might have low enough sensitivities to be undetectable with the finite difference scheme were already screened out by the Morris procedure. Therefore, all parameters in θ_{sens} were retained for subset selection. The resulting parameter set used for subset selection, θ_{sub} , is that initially used for local analysis θ_{sens} :

$$\theta_{sub} = \{\text{TLC}, k, R_u, \nu, A_{mus}, R_s, d_w, d_F, c_F, V_{c,max}, R_{ve}\}. \quad (16)$$

These characterize the total lung capacity, lung elasticity, upper airway resistance, chest wall relaxation volume, driving pressure amplitude, small airway resistance, chest wall compliance, lung recruitment range, mean opening lung pressure, collapsible airway volume, and lung viscoelastic resistance.

Table 7: Relative sensitivity rankings of the θ_{sens} parameter set for treated and deficient lung scenarios against combined and individual airflow \dot{V} and pleural pressure P_{pl} states.

		TLC	k	R_u	ν	A_{mus}	R_s	d_{cw}	$V_{c,max}$	R_{ve}	d_F	c_F
Treated	$P_{pl} \ \& \ \dot{V}$	1	2	3	4	5	6	7	8	9	10	11
	P_{pl}	5	2	7	1	3	9	4	6	8	10	11
	\dot{V}	1	2	3	9	5	4	6	10	8	7	11
Deficient	$P_{pl} \ \& \ \dot{V}$	1	5	7	8	3	9	6	10	11	4	2
	P_{pl}	5	7	9	3	1	10	2	6	11	8	4
	\dot{V}	1	4	6	9	5	7	8	10	11	3	2

5.5. Identifiability

The SVD-based method was applied as described in Section 44.3 to the individual and combined airflow and pleural pressure outputs, given that both outputs contribute to overall model sensitivity. A subset $\tilde{\theta}_{sub,\rho}^*$ was generated for treated and deficient lung scenarios separately and for each clinical data scenario. The method identified eight parameters as identifiable for the deficient lung, but only seven for the treated lung, with the combined model outputs P_{pl} and \dot{V} generally constructing a viable subset by taking the union of the subsets associated with the individual model outputs (see Table 8). The four non-identifiable parameters in the treated scenario are mean opening lung pressure c_F , small airway resistance R_s , upper airway resistance R_u and muscle pressure amplitude A_{mus} , whereas non-identifiable parameters for the deficient lung are lung elasticity k , upper airway resistance R_u , and viscoelastic resistance R_{ve} . Resistance R_u is likely non-identifiable due to it appearing in series with, and thus sharing a dependence with, R_s . Parameters k , A_{mus} in the treated lung and ν , d_{cw} in the deficient lung displayed subset inclusion solely for either combined or individual model outputs, possibly due to interaction between weaker

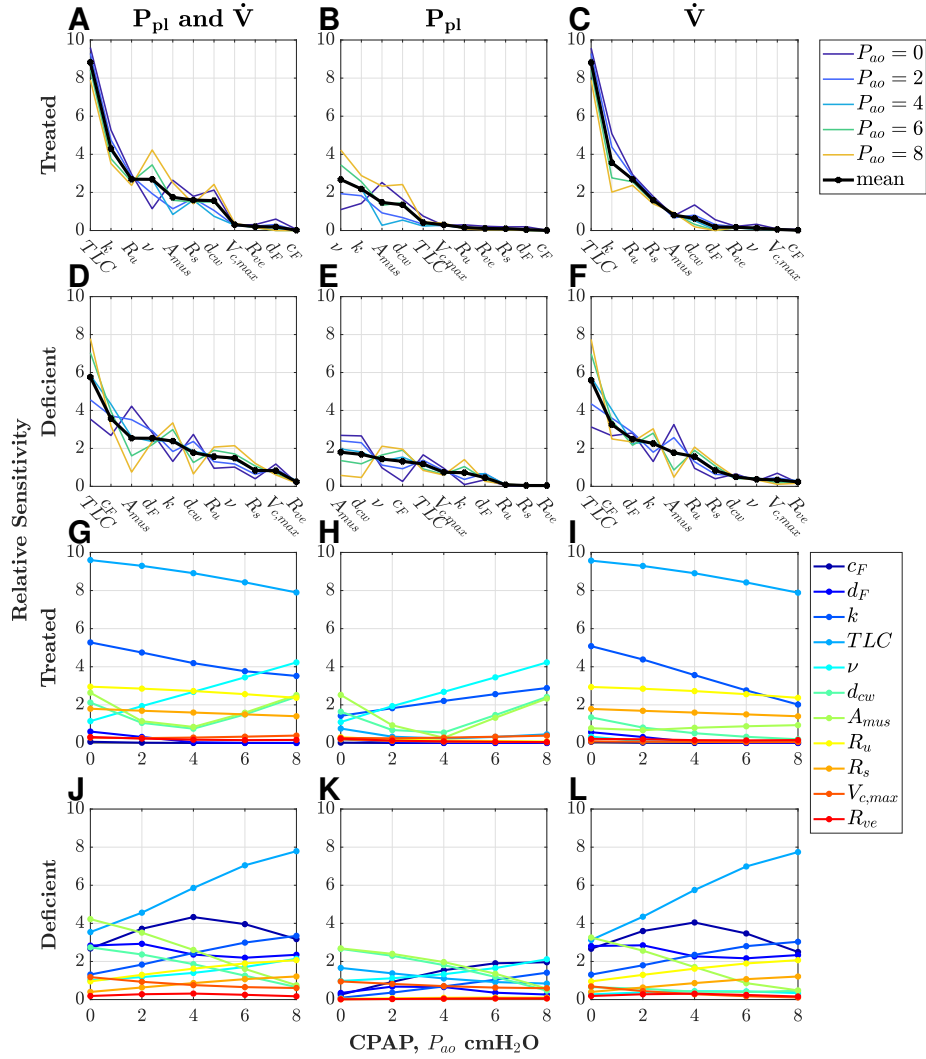


Figure 4: Relative local sensitivities of the parameter set θ_{sens} shown in decreasing mean sensitivity across 5 levels of CPAP. Simulated scenarios include the surfactant treated (panels A-C) and deficient (panels D-F) lungs with associated nominal parameter values. Panels G-L display relative local sensitivities against CPAP level for each parameter in θ_{sens} . Model outputs of interest during local sensitivity analysis include combined pleural pressure P_{pl} and airflow \dot{V} signals (left), and the individual states P_{pl} (middle) and \dot{V} (right). Administered CPAP is simulated via parameter P_{ao} , which is measured in cmH_2O units.

parameters or each other. Taking a less restrictive approach towards a final identifiable subset θ_{opt} for optimization, all parameters in θ_{sub} except R_u are candidates for optimization:

$$\theta_{opt} = \{\text{TLC}, k, \nu, A_{mus}, R_s, d_w, d_F, c_F, V_{c,max}, R_{ve}\}. \quad (17)$$

Table 8: Singular value decomposition based parameter subset selection on θ_{sub} with respect to \dot{V} , P_{pl} , and combined model outputs, for surfactant-treated and deficient lung scenarios. **X** denotes inclusion in the parameter subset.

		TLC	k	R_u	ν	A_{mus}	R_s	d_{cw}	d_F	c_F	$V_{c,max}$	R_{ve}
Treated	P_{pl} & \dot{V}	X	X		X			X	X		X	X
	P_{pl}	X			X	X			X			X
	\dot{V}	X			X	X		X	X		X	
Deficient	P_{pl} & \dot{V}	X			X	X	X	X	X	X	X	
	P_{pl}	X				X			X	X		
	\dot{V}	X				X	X		X	X	X	

5.6. Parameter estimation

Table 9: Nominal and optimized parameter values for parameter set θ_{opt} against airflow and pleural pressure data sets extracted from [28]. Nominal starting values for the treated and deficient lung scenarios are given to initialize the L-M optimization procedure outlined in section 4.5. Both starting parameter sets converged to the optimal parameter values in the last row. Units are listed in Table 3. Bolded, italicized values indicate the parameter attained its upper constraints; italicized plain text values indicate it attained its lower constraint.

	TLC	k	ν	A_{mus}	R_s	d_{cw}	d_F	c_F	$V_{c,max}$	R_{ve}	Cost
Treated	63	0.07	0.25	1.85	12	0.48	0.5	0.1	2.5	20	16.771
Deficient	53	0.04	0.25	1.85	12	0.48	3	8	2.5	20	36.48
Optimal	73	0.044	0.28	3.24	18	1.43	<i>0.5</i>	2.28	3.0	13.09	2.092

Parameter set θ_{opt} was optimized against clinically recorded airflow and pleural pressure signals extracted from Abbasi and Bhutani (1990) [28], using the constrained Levenberg-Marquardt algorithm described in Section 4.5. Optimization was performed separately using the treated and deficient lung scenarios (see Tables 3,5) as two distinct nominal parameter sets, and both initial parameter estimates converged to the same optimal values. Optimization constraints were set according to the Morris bounds in Table 6. Optimized parameter values were found to be within reasonable physiological ranges, as discussed when constructing the Morris bounds in Section 4. When optimizing the entire parameter set θ_{opt} , all parameter values except lung elasticity k and viscoelastic resistance

R_{ve} increased from their nominal treated lung values. Of special notice are total lung capacity TLC, chest wall relaxation volume ν , small airway resistance R_s , lung recruitment range coefficient d_F , and maximum collapsible airway volume $V_{c,max}$, all of which attained either their higher or lower constraints set by the Morris bounds. Optimized θ_{opt} values were found to incorporate attributes of both lung health scenarios, with higher TLC and lower d_F reflecting a more treated lung, and lower k and higher c_F reflecting a more deficient lung. The implications of the constraints on data fitting and potential insights on patient-specific health attributes obtained from optimization results are considered in the Discussion.

Figure 5 reports model outputs (A,C) and normalized residual (B,D) plots with nominal and optimized parameter values against clinical data during spontaneous breathing. Model outputs generated by the optimized parameter set θ_{opt} produced airflow ranging between -28.60 and 31.97 ml/s and pleural pressure between -6.58 and -1.76 cmH₂O, both of which represent the ranges in the data set. Airflow and pleural pressure residuals were normalized by their corresponding maximum absolute data values during the optimization scheme to maintain a common scale and discourage the optimizer from favoring one of the model outputs. The normalized residual plot was selected instead of the typical residual to highlight the inner mechanisms of the optimization structure. Normalized residuals were smaller for both optimized model outputs with the exceptions of the 0.7-0.13 and 0.77-0.95 period time frames when the nominal parameter set fits closer to data than the optimal set in the airflow data scenario, likely due to smaller reported airflow during exhalation.

Figure 6 shows chest wall, lung, and total respiratory pressure-volume relations with treated and deficient lung (see Tables 3, 5) and optimal parameter scenarios (Table 9). The treated lung scenario in Figure 6A reported a tidal volume of 6.00 ml and respective breath-to-breath dynamic lung $C_{l,dyn}$ and chest wall $C_{cw,dyn}$ compliances of 2.56 ml/cmH₂O and 10.09 ml/cmH₂O, which match expected values listed in Table 4. Spontaneous inhalation starts on the tidal loop at an a FRC of 25.1 ml at a low elastic lung pressure of 1.046 cmH₂O. The deficient lung scenario depicted in Figure 6B reported a severely suppressed tidal volume of 0.96 ml and lower $C_{l,dyn}$ and $C_{cw,dyn}$ values of 0.30 ml/cmH₂O and 3.12 ml/cmH₂O, respectively. Deficient lung parameters found in Table 5 pushed tidal breathing into a lower volume regime, with spontaneous breathing starting close to an FRC of 23.2 ml at a higher lung pressure of 1.807 cmH₂O compared to a treated lung. The optimized model scenario shown in Figure 6C reported model outputs similar to those in the treated lung case, with an increased tidal volume of 8.81 ml and dynamic lung compliance $C_{l,dyn}$ of 2.39 ml/cmH₂O. The optimal model further reported a dynamic chest wall compliance of 4.74 ml/cmH₂O, which is more representative of the deficient lung case. Spontaneous breathing with optimal parameter values began in a higher pressure regime compared to the treated and deficient lung scenarios, with a reported FRC of 26.2 ml at an associated lung pressure of 2.51 cmH₂O.

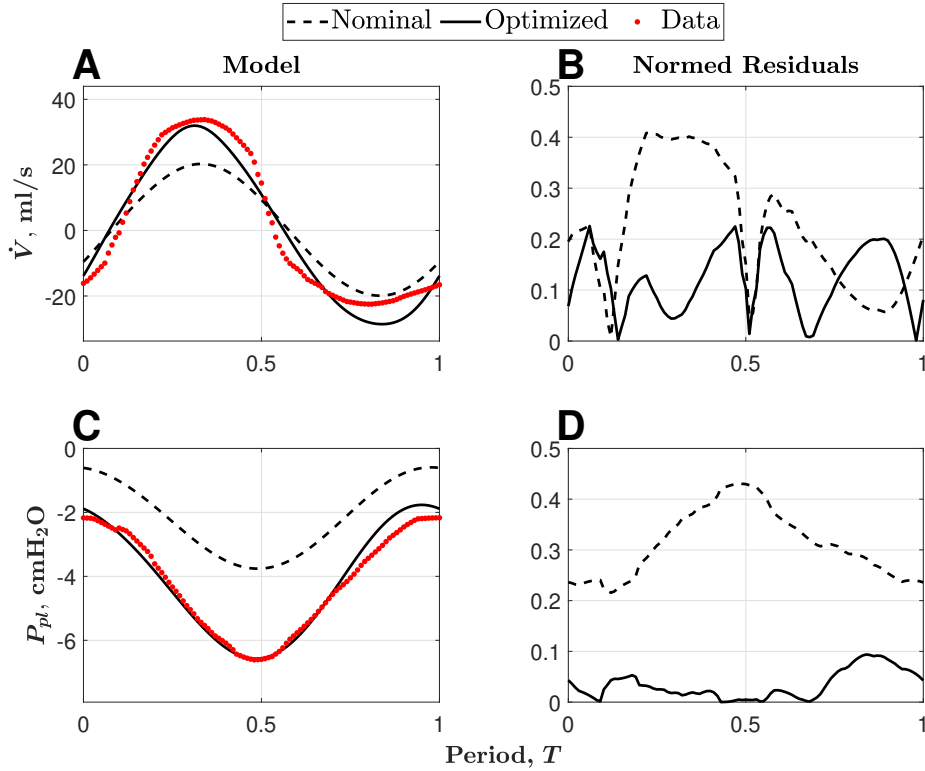


Figure 5: Model outputs generated by nominal treated and optimal parameter sets θ and θ_{opt} during spontaneous breathing. A constrained Levenberg-Marquardt optimization scheme with physiologically-informed bounds was applied to the parameters in θ_{opt} against clinically recorded signals of airflow \dot{V} and pleural pressure P_{pl} . Highlighted data in panels A and C were extracted from waveforms in [28]. Panels B,D: Residuals for \dot{V} and P_{pl} were independently normalized by maximum absolute airflow and pleural pressure to maintain optimization on a single scale.

6. Discussion

This study presented an analysis of the parameter space of a dynamic respiratory mechanics model adapted to the extremely preterm low birthweight infant. In particular, the effects of lung health and simple ventilation support on conventional clinical data tracings were analyzed. Results showed that the combined approach of global screening and local sensitivity and identifiability techniques reduced both the model and the parameter space, to allow prediction of airflow and pleural pressure in a stabilized non-ventilated 1 kg infant.

The Morris screening was useful for exploring parameter ranges that varied greatly depending on the parameter. As examples, a wide range was set for P_{ao} that encompassed possible clinical settings for CPAP [44], and a tight range for ν knowing where the chest wall pressure-volume curve crosses the volume axis [61]. However, the screening had the freedom to choose parameter combinations

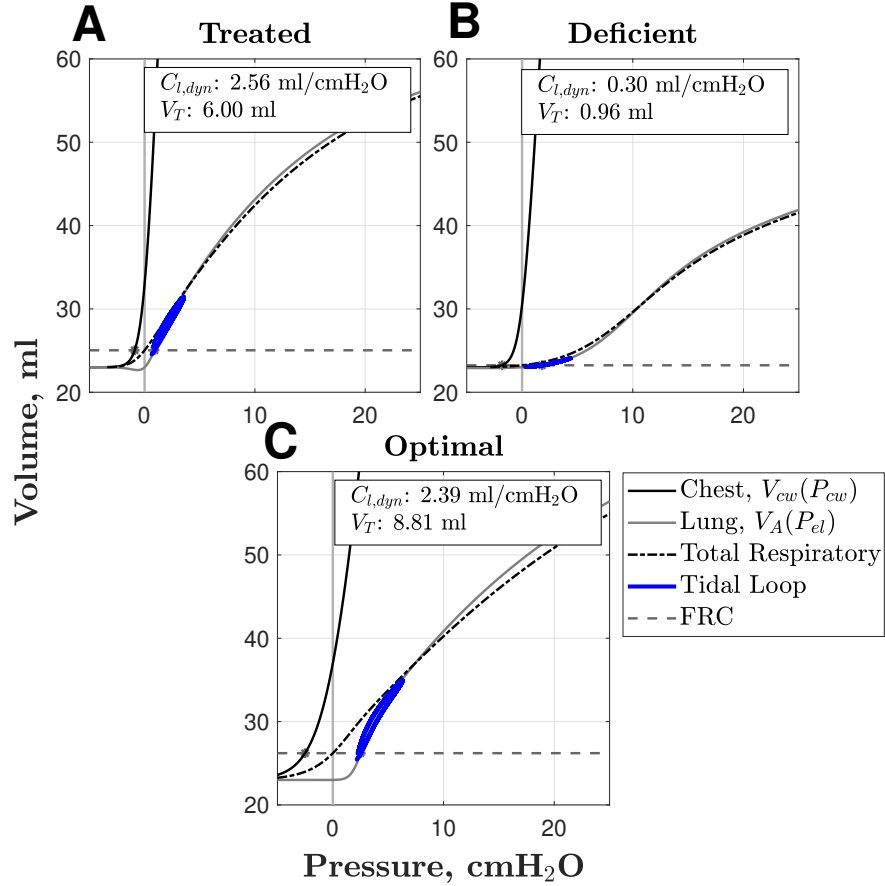


Figure 6: Static pressure-volume relations and tidal breathing loops of the chest wall $V_{cw}(P_{cw})$, lungs $V_A(P_{el})$, and total respiratory system for the reduced model under nominal treated (A), deficient (B), and optimal (C) parameter values. Total respiratory system compliance is generated by the pressure-wise sum of the chest wall and lungs. FRC is determined by the total respiratory system volume when chest wall and lung pressures balance atmospheric pressure, or when the respiratory system pressure is zero. The superimposed blue loop portrays the tidal breathing loop, defined as dynamic $V_A(P_{el} + P_{ve})$. Formulas for dynamic lung compliance $C_{l,dyn}$ and tidal volume V_T are found in Section 22.32.3.1. Optimal parameter values for panel C were obtained in the parameter estimation scheme detailed in Section 44.5

that were non-physiological and would not computationally proceed (e.g. an alveolar volume below residual volume would lead to undefined calculations). This was addressed by customizing the Morris code to restart a new search curve when the model would not run. It is possible that the algorithm was inherently less randomized as a result, however given that there were 1000 runs performed,

it is more likely that the parameter space was spanned enough for reasonable screening results. Determining the effect of removing problematic runs would be a possible point of future investigation.

As respiratory mechanics models have grown in complexity over the decades [62, 4, 5], more physiological and pathological conditions have been able to be simulated and investigated computationally. However, the same complexity can obscure which model components are critical to describe the dynamics of interest and potentially add needless computational time. For example, some of the nonlinearity originally in the current model was adapted from a study characterizing the forced vital capacity maneuver which incorporates breathing up to TLC [3], but the preterm infant would be breathing only at standard tidal volumes. Considering the purpose of any model allows for only including components and parameters directly related to the outputs under study. The model streamlining and reduction in this study using parameter ranges related to lung health and ventilation allowed for the removal of unnecessary nonlinearity which aided in the parameter identifiability afterwards.

Sensitivity analysis showed that despite normalizing the simulated model outputs, airflow was the greater contributor to sensitivity than the pleural pressure. The parameters characterizing the capacity of the lung, TLC and k , were sensitive in both states of lung health. The driving pressure amplitude was a large contributor as well, but more so for pleural pressure than airflow. Additionally, the parameters characterizing the opening ability of the lung were more sensitive when those parameters were higher, signifying a higher pressure and range of pressures needed to open alveoli. The resulting change in the pressure-volume curve of the lung directly impacted the nature of the tidal loop (see Fig. 6). The upper airway resistance had a larger impact in a treated lung, but less so in the deficient lung where it appeared the lung parameters took over.

The dependence on CPAP levels was highlighted more strongly in the deficient lung, where several parameters such as the resistances had higher sensitivity under no ventilation but then immediately dropped in sensitivity once mild CPAP was applied. Very little of this effect was seen in the pleural pressure, but more strongly in the airflow. Since the deficient lung had much higher opening pressures, it is possible that under no ventilation, the dynamic lung compliance was low (flat pressure-volume curve) which favors the impact of factors external to the lungs, but moving to the "midpoint" of the curve increased dynamic compliance and favored the impact of lung parameters. The decreases of sensitivities of TLC and k with respect to volume in the treated lung but increases in the deficient lung align with this theory. The unusual dip in sensitivity of the muscle driving pressure and chest wall compliance with respect to pleural pressure may also be related to changes in lung compliance along the pressure-volume curve, as this is not seen in the deficient case.

Even though non-influential parameters were eliminated early in the parameterization stage of model development, they still provide information about model components. Prime examples include the collapsible airway parameters c_c , d_c , and K_c . The physiological analog is likely that preterm infant breathing occurs generally with small tidal volumes and airflow, pushing the typically

nonlinear volume-resistance relationship of the collapsible airways into a linear regime. In a global screening method such as the Morris method employed here, linear relationships between parameters would likely reduce their associated elementary effect variances and consequently, their Morris indices. In practice, most other resistance-related parameters such as R_{sm} , R_{sd} , K_s , and K_u were globally screened as non-influential likely due to similar reasons. In a small neighborhood of volume and airflow, resistances might be better represented by a linear relationship. Moreover, subset selection results found that constant R_u and R_s exhibited enough dependency to warrant the further use of only one resistance in the parameter optimization process. During local analysis, mean opening lung pressure c_F and lung pressure range d_F were insensitive towards model outputs when given treated lung values, likely since small changes in healthy lung compliance would not drastically change functional residual capacity or tidal breathing characteristics. On the other hand, c_F and d_F values associated with the deficient lung would greatly alter lung pressure at functional residual capacity and dynamic lung compliance in the tidal loop, thus directly affecting the location and magnitude of tidal breathing in pressure-volume space and likely lowering airflow in the upper airways.

Patient-specific optimization results indicated that it is feasible for this model to identify characterizing parameter values of a non-ventilated 1 kg infant. Tidal volume and dynamic lung compliance of the optimized model are 8.81 ml and 2.39 ml/cmH₂O, near the ranges 7.7 to 8.7 ml and 1.99 to 2.13 ml/cmH₂O respectively of the extracted data and comparable to values reported in Table 4 (see also Fig. 1 of Abbasi and Bhutani)[28]. Several parameter values optimized towards or at the treated end of their ranges, indicating a stronger diaphragm, less compliant and more supportive chest wall, higher TLC, and more homogeneous lung. Conversely, the lung elasticity and mean opening pressure parameters optimized away from the treated end of their ranges, suggesting a stiffer lung that requires a higher pressure to open. One hypothesis might be that there is a systemic challenge with opening alveoli across the lung (perhaps an overall surfactant deficiency), as opposed to a larger range of opening pressures indicating varying levels of health (as may occur with a localized injury or pathology.) Future studies should consider stronger approaches for parameter uncertainty and confidence intervals on sparse clinical data, such as parametric bootstrapping intervals [63, 64]. Estimating model parameters against synthetic data created from simulated model realizations with an added noise structure reflecting measurement error may help address the absence of clinical data altogether [46, 17, 65].

We noted that some parameters reached their constraints, suggesting that looser constraints might allow for mathematically more accurate parameter estimates. However this must be viewed in light of the model assumptions which could point to further model assessment needed. Regarding lung volume, TLC increases the maximum and k increases the speed at which it reaches the maximum (higher k means higher volumes at lower elastic recoil pressures). In the optimization, TLC reached its upper constraint but k decreases towards its lower constraint, suggesting the maximum lung volume could be larger but it

will be reached slowly. A constraint on TLC should be determined in light of possible physiology, e.g. with a nominal value of 63 ml it would not be expected to double in this population. Finally regarding lung pressure, the value for opening pressure range d_F optimized at its lower constraint, suggesting that it might naturally want to be lower. However this would suggest an even tighter range of opening pressures when mean opening pressure is non-negligible at 2.28 cmH₂O. It is more likely that a portion of the lung would have higher opening pressures, raising the mean and the range of pressures and reflected by a less steep sigmoidal curve. This constraint was lowered to test the viability of a steeper curve, but caused computational errors from non-physiological scenarios related to the above.

Several features of preterm infant respiratory mechanics are not yet captured by the model and may be contributing to the data fit, particularly the sinusoidal driving pressure function. These include variable frequency of breathing, non-sinusoidal respiratory muscle pressure, intermittent deep breathing (sighing), variable time spent in inspiration vs. expiration, and chemoreflex feedback. Currently the simplest continuous periodic function that does reasonably well emulating breathing in infants is used to drive the model. The data does show a slightly uneven inspiration/expiration ratio, and not purely sinusoidal shape, which could be easily modeled with a different piecewise continuous periodic function. A variety of driving functions have been used to model breathing [5, 29] and could be used here, though they would increase the parameter space for identifiability. Possible parameter dependencies as described above should still be explored further for different model assumptions or physiological scenarios.

This study focused on global one-at-a-time screening, local differential sensitivity analysis, SVD-based subset selection, and gradient-based optimization for parameter identification. Performing these analyses with two lung health scenarios and five levels of pressure support ventilation explores the issues surrounding the sensitivity of model output to vastly different parameter values in the viable parameter space for the system. There are numerous approaches available to study parameter identification and estimation with optimization that were not used in this study. Many studies approach global analysis as a repeated local analysis using random uniform or Latin hypercube sampling [66, 16]. The global Morris screening used here is considered an extension of the local analyses and performs more efficiently, making it a reasonable choice for a system with a large parameter space. This could be extended more globally by the calculation of Derivative-based global sensitive measures [52]. Variance-based methods such as the Sobol method and eFAST were not explored, and could add more information, though they are computationally more expensive than the derivative-based methods. Olufsen and Ottesen [67] compare parameter identifiability of a model of heart rate regulation using a structured correlation method, the SVD method, and model Hessian subspace method. Their work found the structured correlation method to produce the “best” subset with fewest interdependent parameters, and the SVD method did not give as precise parameter estimates but is much more computationally feasible. Of course the above methods assume deterministic model behavior, but physiological phenomena are stochastic process

and may not be as well suited for frequentist techniques. If more probabilistic information about the model is known, methods such as maximum likelihood estimation and Bayesian inference may be considered for future studies [18, 46].

The clinical applicability of these analyses is directly related to both the available data and the model construction. As seen in Abbasi and Bhutani [28], lung volume V_A can be a piece of clinically available data, but is recorded as volume relative to FRC instead of an absolute lung volume and in the model is simply integrated airflow. Any breath-to-breath changes in FRC are not captured in this data. Though it was not reasonable to compare the dynamic absolute V_A , model tidal volume was used as a scalar output for the Morris screening and could be added to the output vector for parameter estimation against clinical data. It is important to reiterate that we estimated parameters responsible during stable breathing without any ventilation or respiratory distress. Possible effects of other parameters, such as significant airway obstruction represented by high resistances, are not captured by the Morris screening due to the limits on the bounds. A future translational approach could follow what has been done by Kretschmer et al [68], who compared model-based parameter estimation with a standard clinical method to determine compliances and resistances under several respiratory maneuvers. From a different perspective, if a parameter determined to be non-identifiable was also deemed clinically relevant, this could motivate collection of new experimental data.

7. Conclusion

Respiratory mechanics models have been investigated increasingly in recent years. This study investigated the use of practical identifiability and parameter estimation techniques in a lumped-parameter respiratory mechanics model of a spontaneously breathing preterm infant, a demographic that is challenging to study experimentally and has limited data. The model first demonstrates the effects of CPAP administration in surfactant-treated and surfactant-deficient lung scenarios before undergoing global and local sensitivity analyses and model reduction via singular value decomposition and QR-factorization subset selection. A reduced model was achieved primarily by linearizing resistive relations. Optimization was performed against clinical waveforms of airflow and pleural pressure data, resulting in plausible interpretation of individual patient physiology. Results gave a sensitive identifiable parameter subset that may elucidate differences between states of lung health when evaluated using optimization against a clinical data set. These methods may be applied to future data obtained clinically under a variety of states of health and ventilation modalities to estimate patient-specific parameters that may help uncover factors leading to respiratory distress. Future work in the scope of providing parameter uncertainty quantification and responses to adverse clinical scenarios would further inform on possible interventions in a clinical setting. The ability to predict respiratory distress could lead to prevention strategies and assist in the health and stability of the preterm infant population.

Data Availability

Source code that generates model structure and nominal model outputs can be found at <http://www.doi.org/10.5281/zenodo.14623545>. Code pertaining to other processes described in the current study can be made available upon request.

Conflicts of Interest

The authors declare no conflicts of interest.

Acknowledgments

This research was supported in part by the Atlantic Pediatric Device Consortium FDA grant 5P50FD004193-07.

References

- [1] Golden JF, Jr. JWC, Stevens PM. 1973 Mathematical modeling of pulmonary airway dynamics. IEEE Trans Biomed Eng **20**, 397–404.
- [2] Verbraak AFM, Bogaard JM, Beneken JEW, Hoorn E, Versprille A. 1991 Serial lung model for simulation and parameter estimation in body plethysmography. Med and Biol Eng and Comput **29**, 309–317.
- [3] Liu CH, Niranjana SC, Jr. JWC, San KY, Swischenburger JB, Bidani A. 1998 Airway mechanics, gas exchange, and blood flow in a nonlinear model of the normal human lung. J Appl Physiol **84**, 1447–69.
- [4] Athanasiades A, Ghorbel F, Jr. JWC, Niranjana S, Olansen J, Zwischenberger JB, Bidani A. 2000 Energy analysis of a nonlinear model of the normal human lung. J Biol Sys **8**, 115–139.
- [5] Le Rolle V, Samson N, Praud JP, Hernandez AI. 2013 Mathematical modeling of respiratory system mechanics in the newborn lamb. Acta Biotheor **91**, 91–107.
- [6] Ellwein Fix L, Khoury J, Moores RR, Linkous L, Brandes M, Rozycki H. 2018 Theoretical open loop model of respiratory mechanics in the extremely preterm infant. PLoS ONE **13**, 1–22. (10.1371/journal.pone.0198425)
- [7] Love WG, Tillery B. 1953 New treatment for atelectasis of the newborn. AMA J Dis Child **86**, 423–425.
- [8] Beltrand J, Alison M, Nicolescu R, Verkauskiene R, Deghmoun S, Sibony O, Sebag G, Levy-Marchal C. 2008 Bone mineral content at birth is determined both by birth weight and fetal growth pattern. Pediatr Res **64**, 86–90.

- [9] Kovacs CS. 2015 Calcium, phosphorus, and bone metabolism in the fetus and newborn. Early Hum Dev **50**, 623–628.
- [10] Manley BJ, Owen LS, Doyle LW, Andersen CC, Cartwright DW, Pritchard MA, Donath SM, Davis PG. 2013 High-flow nasal cannulae in very preterm infants after extubation. N Engl J Med **369**, 1425–1433.
- [11] Bhandari V. 2013 The potential of non-invasive ventilation to decrease BPD. Semin Perinatol **37**, 108–114.
- [12] Siew ML, van Vonderen JJ, Hooper SB, te Pas AB. 2015 Very preterm infants failing CPCP show signs of fatigue immediately after birth. PLoS ONE **10**, 1039–1051.
- [13] Eslami M. 1994 Theory of sensitivity in dynamic systems: an introduction. Berlin: Springer-Verlag.
- [14] Karnavas WJ, Sanchez PJ, Bahill AT. 1993 Sensitivity analyses of continuous and discrete systems in the time and frequency domains. IEEE Trans Syst Man Cybern **23**, 488–501.
- [15] Sher AA, Wang K, Wathen A, Maybank P, Mirams G, Abramson D, Noble D, Gavaghan D. 2013 A local sensitivity analysis method for developing biological models with identifiable parameters: Application to cardiac ionic channel modelling. Future Gener Comput Syst **29**, 591–598.
- [16] Olsen C, Ottesen J, Smith R, Olufsen M. 2019 Parameter subset selection techniques for problems in mathematical biology. Biol Cybern **113**, 121–138.
- [17] Roosa K, Chowell G. 2019 Assessing parameter identifiability in compartmental dynamic models using a computational approach: application to infectious disease transmission models. Theor Biol Med Model **16**, 1.
- [18] Y-H. Kao ME. 2018 Practical unidentifiability of a simple vector-borne disease model: Implications for parameter estimation and intervention assessment. Epidemics **25**, 89–100.
- [19] Lutchen KR, Saidel GM. 1986 Estimation of mechanical parameters in multicompartment models applied to normal and obstructed lungs during tidal breathing. IEEE Trans Biomed Eng **BME-33**, 878–887.
- [20] Avanzolini G, Barbini P, Cappello A, Cevenini G, Chiari L. 1997 A new approach for tracking respiratory mechanical parameters in real-time. Ann Biomed Eng **25**, 154–163.
- [21] Saatci E, Akan A. 2008 Respiratory parameter estimation in linear lung models. Conf Proc IEEE Eng Med Biol Soc **2008**, 307–310.

- [22] Schranz C, Knoebel C, Kretschmer J, Zhao Z, Moeller K. 2011 Hierarchical parameter identification in models of respiratory mechanics. IEEE Trans Biomed Eng **58**, 3234.
- [23] Schranz C, Docherty PD, Chiew YS, Moeller K, Chase JG. 2012 Iterative integral parameter identification of a respiratory mechanics model. Biomed Eng Online **11**, 1–14.
- [24] Schranz C, Docherty PD, Chiew YS, Chase JG, Moeller K. 2011 Structural identifiability and practical applicability of an alveolar recruitment model for ARDS patients. IEEE Trans Biomed Eng **58**, 3234.
- [25] Al-Omar C, Le Rolle V, Pladys P, Samson N, Hernandez A, Carrault G, Praud JP. 2019 Influence of nasal CPAP on cardiorespiratory control in healthy neonate. J Appl Physiol pp. 1370–1385.
- [26] Foster RR, Smith B, Ellwein Fix L. 2023 Thoracoabdominal asynchrony in a virtual preterm infant: computational modeling and analysis. Am J Physiol Lung Cell Mol Physiol **325**, L190–L205.
- [27] Luke R, Kelly G, Stoner M, O’Brien J, Lubkin S, Fix LE. 2024 Towards a Mathematical Understanding of Ventilator-Induced Lung Injury in Preterm Rat Pups. In R. Segal, B. Shtylla SS, editor, Mathematical Modeling for Women’s Health: Collaborative Workshop for Women in Mathematical Biology, pp. 167–211. Cham: Springer Nature Switzerland.
- [28] Abbasi S, Bhutani V. 1990 Pulmonary Mechanics and Energetics of Normal, Non-Ventilated Low Birthweight Infants. Pediatr Pulmonol **8**, 89–95.
- [29] Albanese A, Cheng L, Ursino M, Chbat N. 2016 An integrated mathematical model of the human cardiopulmonary system: model development. Am J Physiol Heart Circ Physiol **310**, H899–H921.
- [30] Hamlington KL, Smith BJ, Allen GB, Bates JHT. 2016 Predicting ventilator-induced lung injury using a lung injury cost function. J Appl Physiol **121**, 106–114.
- [31] Smith C, Nelson N. 1976 The physiology of the newborn infant. Springfield, IL: Thomas.
- [32] Donn SM. 1998 Neonatal and Pediatric Pulmonary Graphics. Armonk, NY: Futura Publishing Company.
- [33] Mortola JP. 1987 Dynamics of breathing in newborn mammals. Physiol Rev **67**, 187–243.
- [34] Singh R, Courtney SE, Weisner MD, Habib RH. 2012 Respiratory mechanics during high-frequency oscillatory ventilation: a physical model and preterm infant study. J Appl Physiol **112**, 1105–1113.

- [35] Neumann RP, Pillow JJ, Thamrin C, Larcombe AN, Hall GL, Schulzke SM. 2015 Influence of gestational age on dead space and alveolar ventilation in preterm infants ventilated with volume guarantee. Neonatology **107**, 43–49.
- [36] Ratjen FA, Wiesenmann HG. 1992 Variability of dynamic compliance measurements in spontaneously breathing and ventilated newborn infants. Pediatr Pulmonol **12**, 73–80.
- [37] Ferreira JC, Bensenor FEM, Rocha MJJ, Salge JM, Harris RS, Malhotra A, Kairalla RA, Kacmarek RM, Carvalho C. 2011 A sigmoidal fit for pressure-volume curves of idiopathic pulmonary fibrosis patients on mechanical ventilation: clinical implications. Clinics **66**, 1157–1163.
- [38] Goldsmith JP, Karotkin EH. 2011 Assisted Ventilation of the Neonate. ClinicalKey 2012. Elsevier/Saunders.
- [39] Gerhardt T, Bancalari E. 1980 Chestwall compliance in full-term and premature infants. Acta Paediatr Scand **69**, 359–364.
- [40] Thomas MR, Rafferty GF, Limb ES, Peacock JL, Calvert SA, Marlow N, Milner AD, Greenough A. 2004 Pulmonary function at follow-up of very preterm infants from the United Kingdom Oscillation Study. Am J Respir Crit Care Med **69**, 868–872.
- [41] Pandit PB, Pyon KH, Courtney SE, England SE, Habib RH. 2000 Lung resistance and elastance in spontaneously breathing preterm infants: effects of breathing pattern and demographics. J Appl Physiol **88**, 997–1005.
- [42] Habib RH, Pyon KH, Courtney SE, Aghai ZH. 2003 Spectral characteristics of airway opening and chest wall tidal flows in spontaneously breathing preterm infants. J Appl Physiol **94**, 1933–1940.
- [43] Schmalisch G, Wilitzki S, Wauer RR. 2005 Differences in tidal breathing between infants with chronic lung diseases and healthy controls. BMC Pediatrics **5**, 36–45.
- [44] Locke R, Greenspan JS, Shaffer TH, Rubenstein SD, Wolfson MR. 1991 Effect of Nasal CPAP on Thoracoabdominal Motion in Neonates With Respiratory Insufficiency. Pediatric Pulmonology **11**, 259–264.
- [45] . 2020 PlotDigitizer: Version 2.6.8. .
- [46] Colebank MJ, Chesler NC. 2022 An in-silico analysis of experimental designs to study ventricular function: A focus on the right ventricle. PLOS Computational Biology **18**, e1010017.
- [47] Campolongo F, Cariboni J, Saltelli A. 2007 An effective screening design for sensitivity analysis of large models. Environmental Modelling and Software **22**, 1509–1518.

- [48] Ipsen I, Kelley C, Pope S. 2011 Rank-deficient nonlinear least squares problems and subset selection. SIAM J Numer Anal **49**, 1244–1266.
- [49] Dadashova K, Smith R, Haider M. 2024 Local Identifiability Analysis, Parameter Subset Selection and Verification for a Minimal Brain PBPK Model. Bulletin of Mathematical Biology **86**, 1–30.
- [50] Morris MD. 1991 Factorial sampling plans for preliminary computational experiments. Technometrics **33**, 161–174.
- [51] Saltelli A, Ratto M, Andres T, Campolongo F, Cariboni J, Gatelli D, Saisana M, Tarantola S. 2008 Global sensitivity analysis: the primer. John Wiley & Sons.
- [52] Qian G, Mahdi A. 2020 Sensitivity analysis methods in the biomedical sciences. Mathematical biosciences **323**, 108306.
- [53] Smith RC. 2013 Uncertainty quantification: theory, implementation, and applications vol. 12. SIAM.
- [54] Wentworth MT, Smith RC, Banks HT. 2016 Parameter selection and verification techniques based on global sensitivity analysis illustrated for an HIV model. SIAM/ASA Journal on Uncertainty Quantification **4**, 266–297.
- [55] Bahill AT, Latimer JR, Troost B. 1980 Sensitivity analysis of linear homeomorphic model for human movement. IEEE Trans Syst Man Cybern **10**, 924–929.
- [56] Wu WH, Wang FS, Chang MS. 2010 Sensitivity analysis of dynamic biological systems with time-delays. BMC Bioinformatics **11**, S12.
- [57] . 2018 Supplemental Material. <https://wp.math.ncsu.edu/cdg/supplemental-material/>. Accessed: 2018-08-02.
- [58] Pope S, Ellwein L, Zapata C, Novak V, Kelley C, Olufsen M. 2009 Estimation and identification of parameters in a lumped cerebrovascular model. Math Biosci Eng **6**, 93–115.
- [59] Kelley C. 1999 Iterative Methods for Optimization. Philadelphia: Society for Industrial and Applied Mathematics.
- [60] Guttman J, Kessler V, Mols G, Hentschel R, Haberthür C, Geiger K. 2000 Continuous calculation of intratracheal pressure in the presence of pediatric endotracheal tubes. Crit Care Med **28**, 1018–1026.
- [61] Agostini E, Hyatt R. 1986 Static behavior of the respiratory system. In Fishman A, editor, Handbook of Physiology. The Respiratory System. Mechanics of Breathing, part 1 , pp. 113–130. Bethesda, MD: Am Physiol Soc.

- [62] Olender MF, Jr. JWC, Stevens PM. 1976 Analog Computer Simulation of Maximum Expiratory Flow Limitation. IEEE Trans Biomed Eng **23**, 445–452.
- [63] Banks H, Baraldi R, Cross K, Flores K, McHesney C, Poaf L, Thorpe E. 2015 Uncertainty quantification in modeling HIV viral mechanics. Math Biosci Eng **12**, 937–964.
- [64] Chowell G. 2017 Fitting dynamic models to epidemic outbreaks with quantified uncertainty: a primer for parameter uncertainty, identifiability, and forecasts. Infect Dis Model **2**, 379–398.
- [65] Cho H, Lewis A, Storey K, Jennings R, Shtylla B, Reynolds A, Byrne H. 2021 A framework for performing data-driven modeling of tumor growth with radiotherapy treatment. In R. Segal, B. Shtylla SS, editor, Using Mathematics to Understand Biological Complexity: From Cells to Populations, , pp. 179–216. Cham: Springer International.
- [66] Raue A, Schilling M, Bachmann J, Matteson A, Schelke M, Kaschek D, Hug S, Kreutz C, Harms B, Theis F, Klingmüller U, Timmer J. 2013 Lessons learned from quantitative dynamical modeling in systems biology. PLoS ONE **8**, 1–17.
- [67] Olufsen M, Ottesen J. 2012 A practical approach to parameter estimation applied to model predicting heart rate regulation. J Math Biol DOI:10.1007/s00285-012-0535-8, 1–30.
- [68] Kretschmer J, Bibiano C, Laufer B, Docherty P, Chiew Y, Redmon D, Chase J, K.Moller. 2017 Differences in respiratory mechanics estimation with respect to manoeuvres and mathematical models. Biomed Phys Eng Express **3**, 014002.

Appendix A

Implementation of the present model in an in-silico environment will be outlined in this section, with corresponding source code provided in the Data Availability section. Section 4 briefly described the use of the differential equations solver `ode15s` to solve the system in Eq. 1. However, most variables found in system are not described by their own differential equations, but rather by the nonlinear constitutive relations between them, shown primarily in Table 2. For redundancy, the system in Eq. 1 defines the change in states such as airflow \dot{V} , lung elastic recoil pressure P_{el} , collapsible airway volume V_c , and viscoelastic lung pressure P_{ve} , often as functions of different compartment quantities such as transmural pressure P_{tm} , upper airway resistance R_u , and others. Algorithm 1 outlines the explicit process by which the system in Eq. 1 was solved in a computational setting, where time \mathbf{t} , starting time of the breath cycle \mathbf{t}_{prev} , breathing period \mathbf{T} , the vector of state solutions at the previous time point \mathbf{p} ,

and the vector of parameter values `pars` were provided as inputs, and derivative of the states `dpdt` were outputs. This algorithm was used to construct the main function fed through the `ode15s` differential equations solver in MATLAB 2024b, as mentioned briefly in Section 4.

Time-varying solutions to the system in Eq. 1 were obtained from the outputs of the `ode15s` solver, upon which dynamic tracings for all other model states could be calculated by rerunning lines 13-37 of Algorithm 1 in a separate script over the total time span. Further information on the computational architecture of the current model can be found in the available code.

Algorithm 1 dpdt = Model(t,p,T,tprev,parms)

- 1: **Extract parameters** ▷ Example: $c_F = \text{pars}(1)$, $d_F = \text{pars}(2)$
 - 2: $c_F, d_F, k, \text{TLC}, \text{RV}, RR, \nu, c_{cw}, d_{cw}, A_{mus}$
 - 3: $R_{um}, K_u, K_c, R_{sm}, R_{sd}, K_s, I_u, c_c, d_c, V_{c,max}, C_{ve}, R_{ve}, P_{ao}$
 - 4: **Extract state solutions at time t**
 - 5: $\dot{V} = \text{p}(1)$
 - 6: $P_{el} = \text{p}(2)$
 - 7: $V_c = \text{p}(3)$
 - 8: $P_{ve} = \text{p}(4)$
 - 9: **Calculate breathing frequency f and P_{mus}**
 - 10: $f = 1/T$
 - 11: $P_{mus} = A_{mus} \cos(2\pi f(t - t_{prev})) - A_{mus}$ ▷ Diaphragm muscle pressure, P_{mus}
 - 12: **Calculate vital capacity VC and chest wall parameters a_{cw}, b_{cw}**
 - 13: $\text{VC} = \text{TLC} - \text{RV}$
 - 14: $a_{cw} = \text{RV}$
 - 15: $b_{cw} = \frac{\nu \cdot \text{VC}}{\ln(e^{-c_{cw}/d_{cw}} + 1)}$
 - 16: **Calculate alveolar relations**
 - 17: $F_{rec} = \frac{1}{1 + e^{-(P_{el} - c_F)/d_F}}$ ▷ Alveolar recruitment, F_{rec}
 - 18: $V_{el} = \text{VC}(1 - e^{-k \cdot P_{el}})$ ▷ Lung elastic recoil volume, V_{el}
 - 19: $V_A = F_{rec} V_{el} + \text{RV}$ ▷ Alveolar volume, V_A
 - 20: $C_A = \frac{\text{VC} \cdot k \cdot e^{-k \cdot P_{el}}}{e^{-(P_{el} - c_F)/d_F} + 1} - \frac{\text{VC} \cdot e^{-(P_{el} - c_F)/d_F} \cdot (e^{-k \cdot P_{el}} - 1)}{d_F \cdot (e^{-(P_{el} - c_F)/d_F} + 1)^2}$ ▷ Alveolar compliance, C_A
 - 21: **Calculate chest wall relations**
 - 22: $V_{cw} = V_A + V_c$ ▷ Chest wall volume, V_{cw}
 - 23: $P_{cw} = c_{cw} + d_{cw} \cdot \ln(e^{(V_{cw} - a_{cw})/b_{cw}} - 1)$ ▷ Chest wall pressure, P_{cw}
 - 24: **Calculate pressures**
 - 25: $P_{tm} = c_c - d_c \cdot \ln\left(\frac{V_{c,max}}{V_c} - 1\right)$ ▷ Transmural pressure, P_{tm}
 - 26: $P_l = P_{el} + P_{ve}$ ▷ Total pulmonary pressure, P_l
 - 27: $P_{pl} = P_{cw} + P_{mus}$ ▷ Pleural pressure, P_{pl}
 - 28: $P_A = P_l + P_{pl}$ ▷ Alveolar pressure, P_A
 - 29: $P_c = P_{tm} + P_{pl}$ ▷ Collapsible airway pressure, P_c
 - 30: **Calculate resistances**
 - 31: $R_c = K_c \left(\frac{V_{c,max}}{V_c}\right)^2$ ▷ Collapsible airway resistance, R_c
 - 32: $R_s = R_{sd} \cdot e^{\left(K_s \frac{V_A - \text{RV}}{\text{TLC} - \text{RV}}\right) + R_{sm}}$ ▷ Small airway resistance, R_s
 - 33: $R_u = R_{um} + K_u |\dot{V}|$ ▷ Upper airway resistance, R_u
 - 34: **Calculate remaining relations**
 - 35: $P_u = \dot{V} \cdot R_c + P_c$ ▷ Upper airway pressure, P_u
 - 36: $\dot{V}_A = (P_c - P_A)/R_s$ ▷ Alveolar airflow, \dot{V}_A
 - 37: $\dot{V}_c = \dot{V} - \dot{V}_A$ ▷ Collapsible airway flow, \dot{V}
 - 38: **Calculate vector dpdt**
 - 39: $\text{dpdt}(1) = \frac{1}{I_u} \left(P_{ao} - P_u - R_u \dot{V}\right)$ ▷ ODE for \dot{V} , p(1)
 - 40: $\text{dpdt}(2) = \dot{V}_A / C_A$ ▷ ODE for P_{el} , p(2)
 - 41: $\text{dpdt}(3) = \dot{V}_c$ ▷ ODE for V_c , p(3)
 - 42: $\text{dpdt}(4) = (\dot{V}_A - P_{ve}/R_{ve})/C_{ve}$ ▷ ODE for P_{ve} , p(4)
-